Electron collisions with diatomic anions

H. B. Pedersen,[1] N. Djurić,[2] M. J. Jensen,[1] D. Kella,[1] C. P. Safvan,[1] H. T. Schmidt,[3] L. Vejby-Christensen,[1] and L. H. Andersen[1]

[1]*Institute of Physics and Astronomy, University of Aarhus, DK-8000 Aarhus C, Denmark*

[2]*JILA, University of Colorado and National Institute of Standards and Technology, Boulder, Colorado 80309-0440*

[3]*Department of Physics, Atomic Physics, Stockholm University, S-10405 Stockholm, Sweden*

(Received 22 March 1999)

Electron collisions with negative ions (B_2^-, C_2^-, O_2^-, BN^-, and OH) have been performed in a merged-beams experiment at the heavy-ion storage ring ASTRID (Aarhus Storage Ring, Denmark). Absolute cross sections for detachment ($e^- + AB^- \rightarrow AB^0 + 2e^-$) and detachment plus dissociation ($e^- + AB^- \rightarrow A^0 + B^0 + 2e^-$) are reported for energies below 40 eV. For the homonuclear ions, X_2^- ($X = \mathrm{B, C, O}$), cross sections are also presented for dissociative reactions leading to an X^- particle in the final state. The detachment process is dominant for all investigated systems. The detachment cross section is characterized by an effective threshold larger than the electron binding energy. The shapes of the detachment cross sections are similar for the studied anions pointing to a common nonresonant mechanism for detachment. Also, the cross section for detachment plus dissociation and pure dissociation show regularities pointing to a general nonresonant mechanism. Structures are observed in the detachment cross section of C_2^- and BN^- and in the dissociation cross section of B_2^- and C_2^-. The structures are attributed to short-lived dianions (resonances) formed during the collision process. The results are supported by *ab initio* calculations, and it is inferred that electronic excitations are important in the resonant reactions. [S1050-2947(99)05109-4]

PACS number(s): 34.80.Dp, 34.50.Gb, 41.75.Cn

I. INTRODUCTION

We present an experimental investigation of reactive processes in electron-anion scattering using a merged beam setup at the heavy ion storage ring ASTRID (Aarhus Storage Ring, Denmark). The purpose of the experiments is fourfold. We aim to characterize the reaction cross sections at low energy with respect to threshold behaviors, absolute magnitudes, and general energy dependencies. We also aim to investigate the formation and decay of short-lived diatomic dianions as intermediate collision complexes.

Experimentally, the cross sections have been studied for two processes involving detachment of a molecular anion:

$$e^- + AB^- \rightarrow \begin{cases} AB^0 + 2e^-, \\ A^0 + B^0 + 2e^-, \end{cases} \tag{1}$$

where an anion ($AB^- = B_2^-, C_2^-, O_2^-, BN^-, OH^-$) reacts with a free electron (e^-) to produce either the neutral molecule (AB^0) in a *detachment* reaction or two neutral atoms ($A^0 + B^0$) in a *detachment plus dissociation* reaction. For the homonuclear molecular ions (B_2^-, C_2^-, O_2^-), two *dissociation* reactions leading to a negative atomic ion are also considered:

$$e^- + X_2^- \rightarrow \begin{cases} X^- + X^0 + e^-, \\ X^- + X^+ + 2e^-, \end{cases} \tag{2}$$

where X is either B, C, or O.

Electron-anion collisions have been studied experimentally for both atomic [1–15] and molecular systems [16,17]. The long-range Coulomb interaction between the incoming electron and the target anion is evidently an important property, and for weakly bound atomic anions, where the extra electron is bound outside an atomic core, the collision dynamics has been explored in various approximations [18–25]. For molecular systems, where the extra electron often has valence character, the collision dynamics is not clarified. Electron detachment is the dominating break-up reaction which makes electron-anion scattering qualitatively different from electron scattering on neutral or positive molecules where dissociative reactions dominate [26,27].

The stability, structure, and dynamics of doubly charged anions (dianions) have been the subject of substantial experimental and theoretical investigations [28,29]. In this work the formation and decay of short-lived dianions through electron bombardment are addressed, formally written as

$$e^- + AB^- \rightarrow AB^{2-} \rightarrow \text{products}. \tag{3}$$

The question is whether dianionic resonances play a role in electron-anion collisions, and if they do, what are the important decay channels?

This paper is organized as follows. First, previous theoretical and experimental work on electron-anion collisions and dianions is reviewed and discussed. The experimental method is presented in Sec. III. In Sec. IV, *ab initio* calculations performed to support the interpretation of the experimental cross sections are described and discussed. The experimental results are reported together with results of the *ab initio* calculations in Sec. V. The paper ends with a discussion (Sec. VI) and a conclusion (Sec. VII).

II. PREVIOUS INVESTIGATIONS

A. Electron-anion collisions

Experimentally, cross sections for electron impact detachment from negative ions have been measured in crossed

beam experiments for H^- [1–4] and O^- [2]. Inclined beam techniques have been applied for electron impact detachment from H^- [5,6], C^- [7,8], O^- [9,10], and F^- [11] at inclination angles 20° [5] and 10° [6–11]. Before this study, merged beam experiments in heavy ion storage rings have been reported for atomic ions of H^- [12], D^- [13], B^- [14], and O^- [15], plus two molecular ions C_2^- [16,17] and B_2^- [17]. For both atomic and molecular ions, the merged beam technique in storage rings benefits from the long storage time ($\sim$ seconds) that allows for relaxation of electronic and vibrational excitations prior to the actual cross-section measurement, thus providing some control of the initial state [30]. The high beam energy (MeV) achievable in a storage ring combined with the merged beam setup in the so-called electron cooler allows for cross-section measurements at low relative energies with high electron densities ($\sim 10^7\ \mathrm{cm}^{-3}$) and good energy resolution. The dominating process for all previously studied atomic systems is nonresonant electron detachment [12–17]. It has been experimentally established that the detachment cross section is characterized by an effective threshold two to three times the electron binding energy of the anion and a smooth energy dependency above threshold.

Several theoretical descriptions of the atomic detachment process have been reported. Hart *et al.* [18] investigated general properties of the three-body wave function outside a reaction zone and obtained a threshold law which was expected to be valid until 0.4 eV above the energetic threshold. An experimental investigation of this threshold law is difficult with the available techniques since the signal-to-background ratio is highly unfavorable in this region. The importance of the effective threshold was not realized in Ref. [18]. Two-electron models have been applied to describe detachment from atomic anions in classical [19] (both the incoming and bound electrons are described classically), semiclassical [20–23] (the incoming electron is described classically and the bound electron quantum mechanically), and full quantum-mechanical [24,25] (both electrons are described quantum mechanically) approximations. All classical and semiclassical models use the impact parameter formalism where the cross section, $\sigma(E)$, at a given initial electron energy, E, is written as

$$\sigma(E) = 2\pi \int_0^\infty P(E,\rho)\rho\, d\rho. \tag{4}$$

Here $P(E,\rho)$ is the reaction probability and the integration is over the impact parameter, ρ. The reaction probability is hence the subject of the calculations. The physical picture of the detachment reaction implied by the classical and semiclassical approaches relies on the expansion of the electron-electron interaction to first order (the dipole approximation):

$$\frac{1}{|\mathbf{R}-\mathbf{r}|} \approx \frac{1}{R} + \frac{\mathbf{r}\cdot\mathbf{R}}{R^3}, \quad r \ll R, \quad R = |\mathbf{R}|, \tag{5}$$

where $\mathbf{R}$ is the position vector of the incoming electron and $\mathbf{r}$ is the position vector of the bound electron; both are referenced to the center of charge of the anionic system. The first term in the expansion trivially raises the potential of the bound electron, whereas the second term effectively acts as an electrical field on the bound electron. In essence, the detachment reaction is pictured as electric field detachment where the electric field is provided by the incoming electron. In the classical model by Solov'ev [19], the detachment probability is related to the solid angle, $\theta_0(E,\rho)$, through which the bound electron can escape at the distance of closest approach of the incoming electron: $P(E,\rho) = 1 - \cos\theta_0(E,\rho)$. This approach was estimated to be valid for H^- in the energy range $E = 4-20$ eV. Smirnov and Chibisov [20] considered the energies close to threshold for H^-, where classically the bound electron cannot escape. Escape is, however, possible by tunneling through the potential barrier created by the superposition of the potential due to the electric field of the incoming electron and the anionic binding potential. Ostrovsky and Taulbjerg [21] modified the model of Solov'ev by introducing the concept of decay rate (i.e., effectively allowing detachment to occur at any time during the collision) and by assuming the classical model to be valid at small R and the tunneling hypothesis of Smirnov and Chibisov [20] to be valid at large R. The two regions were separated at $R_c \sim 10-13a_0$ for H^-, depending on the model potential used. A semiclassical quantum wave packet simulation of the detachment process was performed by Kazansky and Taulbjerg [22]. They found projectile-induced polarization effects and nonadiabatic features to be important for the detachment reaction. Lin *et al.* [23] calculated cross sections for H^- and O^- using close-coupling theory to describe the bound electron. Lowest-order distorted wave theory was used by Pindzola [24] to describe electron impact detachment from H^- and O^- and reasonable agreement between theory and experiment was found. However, this was considered fortuitous since the importance of polarization effects was regarded as being so significant that higher-order perturbational or nonpertubational methods may be needed for a proper description of the problem. Finally, Robicheaux [25] calculated cross sections for electron impact detachment from H^- and B^- using a T-matrix formalism and an accurate description of the final-state wave function with two electron continua. With this method, good agreement between theory and experiment was obtained and some aspect of the collision dynamics was elucidated.

All two-electron models agree that the long-range Coulomb repulsion, i.e., the distortion of the incoming electron path, is essential in accounting for the effective threshold and the cross section in general. The model of Solov'ev, Smirnov, and Chibisov, and hence the model by Ostrosky and Taulbjerg, and not easily extended beyond detachment of a bound s-wave electron. The various classical and semiclassical theories disagree on the shape of the reaction probability, $P(E,\rho)$ (see, for instance, Fig. 4 of Ref. [22]), thus reflecting different underlying physical aspects of the detachment process, however still rendering cross sections in reasonable agreement with experiment. These models only take weak account of electron correlation between the incoming and the bound electrons, for instance exchange is not considered, and it is a fundamental problem whether a classical description of the incoming electron is valid. The fact that significant target polarization effects are found [22,24] indicates that correlation is indeed important. Thus, a full

quantum-mechanical description seems to be necessary for understanding the actual dynamics of electron-anion collisions [24,25].

A simple qualitative reaction cross section that will be used later to discuss the measured cross section can be obtained within the impact parameter formalism [Eq. (4)] by assuming that $P(\rho,E)$ is a square distribution:

$$P(E,\rho)=\begin{cases} p & \text{if } C(E,\rho)\geqslant 0 \\ 0 & \text{otherwise,} \end{cases} \tag{6}$$

where p is a constant and $C(E,\rho)\geqslant 0$ is some reaction condition. A purely classical reaction condition that has been applied in the case of atomic ions [13] requires the perturbing force of the incoming electron to exceed the binding force on the bound electron. The binding force in a typical negative ion potential is EA/a, where EA is the binding energy and a is the range of the potential. Hence, the reaction condition may formally be stated as

$$\begin{aligned} &\frac{1}{D^2(E,\rho)}-\frac{EA}{a}\geqslant 0 \quad \text{(force condition)}, \\ &D(E,\rho)=\frac{1}{2E}+\left(\frac{1}{(2E)^2}+\rho^2\right)^{1/2}, \end{aligned} \tag{7}$$

where $D(\rho,E)$ is the distance of the closest approach at an initial energy of E. With the condition Eq. (7), the reaction cross section becomes

$$\begin{aligned} &\sigma(E)=p\pi\frac{1}{E_{\rm th}^2}\left(1-\frac{E_{\rm th}}{E}\right), \\ &E_{\rm th}=\left(\frac{EA}{a}\right)^{1/2}. \end{aligned} \tag{8}$$

A semiclassical model [31] uses the condition that the available energy must exceed the energetic threshold at some characteristic reaction distance ($R_{\rm th}$):

$$E-EA-\frac{1}{R_{\rm th}}-\frac{E\rho^2}{R_{\rm th}^2}\geqslant 0 \quad \text{(energy condition)}, \tag{9}$$

where E is the energy of the incoming electron, $1/R_{\rm th}$ is the Coulomb energy lost by the electron at the distance $R_{\rm th}$, and $E\rho/R_{\rm th}^2$ is the centrifugal part of the kinetic energy. Applying this condition [Eq. (9)], the same mathematical form as Eq. (8) is obtained but with a different threshold:

$$\begin{aligned} &\sigma(E)=p\pi R_{\rm th}^2\left(1-\frac{E_{\rm th}}{E}\right), \\ &E_{\rm th}=EA+\frac{1}{R_{\rm th}}. \end{aligned} \tag{10}$$

Both models [Eq. (8) and Eq. (10)] imply effectively a reaction zone of radius $1/E_{\rm th}$ and $R_{\rm th}$, respectively, which the incoming electron must penetrate to cause detachment. Reaction cross sections of the form $\sigma(E)=\sigma_0(1-E_{\rm th}/E)$ are known to reproduce the general energy dependence of detachment cross sections for atomic ions in the threshold region [13–17] (below the cross-section maximum).

B. Dianions

Doubly charged anions (dianions) are common on surfaces, in crystals, and in solutions [32] where the dianion is stabilized by the surrounding host. In the gas phase the stability is governed by either spatial separation of the extra electrons or by delocalization over a part of the nuclear structure. Potential barriers either towards dissociation into charged fragments or towards electron emission will in general exist due to the long-range repulsive Coulomb potential superimposed with a binding potential at shorter range. Stability, structure, formation, and decay of dianions are of fundamental interest in experiment and theory. To characterize dianions, theory must describe the diffuse character of the outer electrons and account for electron correlation. The dynamical aspects, i.e., the formation and decay, are challenging to electron-molecule scattering calculations due to the long-range Coulomb interaction. Recent reviews on dianions have been given by Kalcher and Fox [28] and Scheller *et al.* [29].

The formation of short-lived ($\tau\sim 10^{-16}$–10^{-15} sec) atomic dianions (resonances) is a problem of controversy both experimentally and theoretically. Structures in the detachment cross sections were observed with an inclined beam technique for H^- [5,6] at 14.2 and 17.2 eV, and for O^- [9,10] at 19.5 and 26.5 eV. The structures had widths of ~ 1 eV corresponding to a resonance lifetime of $\sim 10^{-15}$ sec. For H^- the structures were assigned to $(2s^2 2p)^2P$ and $(2p^3)^2P$ by Taylor and Thomas [33,34]. Schnitzer and Anbar [35] observed a state of H^{2-} and D^{2-} in a tandem mass spectrometer, with a half-life of 23 ± 4 nsec. The assignment and the existence of resonances (H^{2-}) were questioned on theoretical grounds by Robicheaux *et al.* [36]. They pointed to the disagreement with a proof by Simon [37] that resonances in any particle system that experiences only Coulomb forces cannot exist above the energy for complete disintegration of the system. For H^- the threshold for complete disintegration is $13.6+0.75=14.35$ eV. Further, they inferred that the modulation of the experimental cross section is inconsistent with the unitarity of the scattering matrix if the assignment of the resonances to be of ^2P character [33,34] holds true. Finally, they used two different types of *ab initio* calculations: (i) a direct calculation of the detachment cross section for low values of the angular momentum using R-matrix methods, and (ii) an estimate of the position of the state $2s^2 2p$ using configuration interaction in a stabilization-type approach. None of these calculations showed evidence for H^{2-} resonances. The resonances calculated by Taylor and Thomas [33,34] were concluded to arise from applying a too small basis set. More recently, merged beam experiments on the ground states of $H^-(1s^2\ ^1S)$ [12] and $D^-(1s^2\ ^1S)$ [13] showed no structures in the cross section for detachment as previously reported [5,6]. Recently, Sommerfeld *et al.* [38,39] predicted a resonance of configuration $(2p^3\ ^4S)$ in H^{2-} using the method of complex rotation to evaluate the resonance energy (~ 1.4 eV above $2p^2\ ^3P$ state of H^-) and width (~ 1.7 eV). The absence of this resonance in the merged beam experiments [12,13] was explained since these

involved electron scattering on ground state $H^-(1s^2\ ^1S)$ and hence the transition to the resonance is spin forbidden. Morishita *et al.* [40] used hyperspherical coordinates and found all adiabatic potential-energy curves of symmetry $^4S^0$ to be repulsive for H^{2-}. This conclusion was also made by Chung [41], who investigated the effects of channel coupling and exchange interactions on the formation of resonances in negative ions. Experimentally, the case of electron scattering on a $2p^2$ configuration was considered for $B^-(2p^2\ ^3P) + e^-$ in a merged beam experiment [14] and no resonances were observed.

Theoretical predictions also exist for resonance dianions of oxygen [36,42–44] and sulfur [36], however no evidence for resonances was seen in a merged beam experiment on $O^-(2p^5\ ^2P)$ [15].

Stability of atomic dianions of O, F, Cl, and Br on a time scale of μsec was first reported in experiments with an omegatron mass spectrometer [45]. The formation of the dianions was speculated to proceed through either electron-anion or anion-anion collisions occurring in the spectrometer. Later, dianions of O, Te, Bi, F, Cl, Br, and I have been observed using a Penning ion source [46]. The findings for I were later attributed to impurities by Frees *et al.* [47], and no evidence for atomic dianions of O, F, Cl, and I was found by Spence *et al.* [48] using a double-focusing mass spectrometer with electron impact and Penning ion sources. In a tandem-accelerator-based charge spectrometer, a search for a series of atomic dianions produced in a cesium sputter ion source with lifetimes $\tau \geqslant 0.1\ \mu$ sec was performed, however no evidence for such species was found [49]. The mass spectroscopy techniques require that the dianions have lifetimes of the order of the transit time in these apparatuses ($\sim 1\ \mu$ sec). Different ion sources have been applied, and some of these may be conditioned for dianion formation and some not. In general, the formation process is not well controlled in such ion sources. To summarize, stable atomic dianions seem to be nonexisting, however dianionic resonances cannot be completely excluded.

A search for a series of diatomic dianions of C_2 and B_2 with lifetimes $\tau \geqslant 0.1\ \mu$sec was also done using a tandem accelerator, and also in this case no evidence for such species was found within the experimental accuracy [50]. There are several theoretical reports on metastable diatomic dianions in the gas phase, in particular BN^{2-} [51–55], C_2^{2-} [51,56–59], and O_2^{2-} [60–64]. The cross sections for electron reactions with C_2^- was investigated in a merged beam experiment [16] and a clear structure was reported at $\sim$10 eV and the structure was assigned to the formation of a dianionic state. The assignment of the structure was addressed by Sommerfeld *et al.* [59] and it was concluded that the structure could not be due to the lowest electronic state of C_2^{2-}.

For larger molecules there are several reports on quasistable dianions. Doubly charged anions C_7^{2-}-C_{28}^{2-} with lifetimes exceeding 10 μsec were produced by sputtering graphite with a 14.5-keV beam of Cs^+ and observed in a double-focusing mass spectrometer [65]. C_{60}^{2-} with a lifetime larger than 1 msec was observed by laser desorption from a surface covered with C_{60} molecules [66]. The stability of C_{60}^{2-} was attributed to a shape resonance resulting from the long-range Coulomb repulsion combined with a short-range electron-anion binding [66,67]. Similarly, the stability of $C_{60}F_{48}^{2-}$ has been attributed to the Coulomb barrier [68]. The experimental conditions for production of doubly charged ions in an ion source are not well defined and hence the information on these species is limited. The question of which is the smallest stable dianion has been addressed by Boldyrev and Simons [51], who suggested Mg_2S^{2-}, and by Scheller and Cederbaum [69,70], who pointed to the metal halides, MX_3^{2-} (M = Li, Na, K; X = F, Cl), some of which has been searched for by accelerator mass spectroscopy (AMS) studies [71]. Many other theoretical characterizations of stable dianions have been reported (see Ref. [28] for an overview).

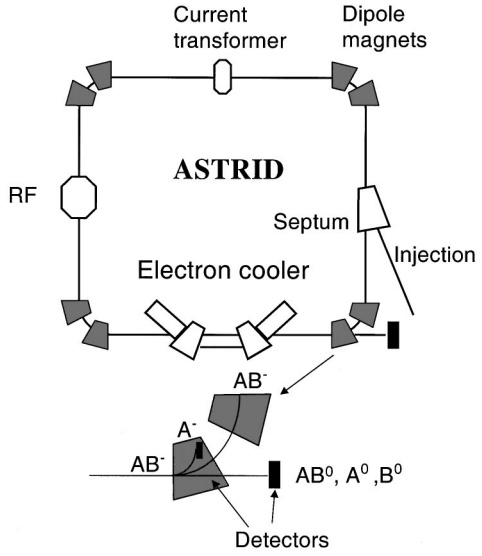

FIG. 1. Schematic drawing of the ASTRID storage ring.

Dynamical studies of the formation and decay of C_{84}^{2-} were performed by Compton *et al.* [72]. Electron attachment was found to occur in the ion source at impact energies 0.5–10 eV and autodetachment from C_{84}^{2-} was observed with a mean lifetime of $\sim$60 μsec. Evidence for dissociative resonances of small carbon clusters C_n^{2-} $n \geqslant 4$, formed by laser ablation of graphite, was found using the covariance mapping technique [73]. No evidence was found for smaller dissociative dianion resonances. Photoelectron spectroscopy on dianions has recently been performed [74,75]. Wang *et al.* [74] studied dianions of the type $^-O_2C(CH_2)_nCO_2^-$ (n = 3–10) and investigated the properties of the repulsive Coulomb barrier and the excess electron binding energy as a function of the equilibrium charge separation.

III. EXPERIMENT

The present series of experiments was carried out at the storage ring ASTRID [76]. The ring is 40 m in circumference, and has a square geometry with two 45° bending magnets in each of the four corners. A schematic drawing of the storage ring is shown in Fig. 1. For production of negative ions (B^-, B_2^-, C_2^-, O_2^-, BN^-, and OH^-) a sputter ion source [77] was used with various sputtering materials. The sputtering material and the typical ion current for the different ions are summarized in Table I. The negative ions were preaccelerated to 150 keV, injected into the storage ring and further accelerated to MeV energies by means of a radiofrequency acceleration system. The storage lifetime of the ion beams was determined by collisions with the residual gas.

TABLE I. Characteristics of the ion beams.

Ion	Sputter material	Ion current	Final energy	Storage lifetime
B_2^-	50% BN+50% Cu	0.5 μA	4.83 MeV	1.5 sec
C_2^-	C (graphite)	5.0 μA	4.98 MeV	1.6 sec
O_2^-	50% Fe_3O_2+50% Cu	0.05 μA	3.76 MeV	1.8 sec
BN^-	50% BN+50% Cu	0.05 μA	4.80 MeV	1.6 sec
OH^-	50% Fe_3O_2+50% Cu	0.10 μA	5.01 MeV	0.5 sec

The gas pressure in the ring was $\sim 3\times 10^{-11}$ mbar. The final energies and storage lifetimes of the ion beams are also shown in Table I. After acceleration, the ions were merged with an essentially monoenergetic electron beam provided by the electron cooler [78,79]. The electron current was 1–3 mA at the cooling energy defined from the matching velocity of ions and electrons. Neutral particles produced in the electron-anion collision process were detected by a 60×40 mm^2 energy sensitive surface barrier detector located behind the dipole magnet following the electron cooler. A grid with transmission probability $T=71\pm 3$ % could be inserted in front of this detector. The grid transmission was measured with B^0 particles emerging from the 2.5-MeV beam of atomic B^-. A horizontally movable 20-mm-diam surface barrier detector was positioned inside the first 45° bending magnet after the electron cooler. With this detector, charged fragments from the electron-ion collision process were detected (see Fig. 1). The electron cooler was operated in a chopping mode. Thus, the electron beam was alternatingly switched on and off at a frequency of typically 20 Hz, and the data-acquisition system was gated to measure the rate of particles with the electron beam on $[R(X)]$ and off $[R_0(X)]$ accordingly. The chopping frequency was kept higher than the inverse vacuum response time ($\sim$10 Hz) to ensure that the pressure was unchanged during measurement of $R(X)$ and $R(X_0)$. The electrostatic pick-up electrodes in the interaction region of the electron cooler were biased with -1.0 V and the clearing electrodes were biased with ± 200 V. With these voltages, excellent agreement between the calculated and experimental value of the space-charge potential was found. The ion current was measured with the bunched ion beam by using a beam charge monitor [80].

Absolute cross sections were obtained with the present experimental setup, since the detection efficiency of the surface barrier detector is unity for particles with MeV energies and all particles emerging from the interaction region were collected. The major uncertainty of the absolute cross sections is associated with the ion current measurement. Relative cross sections are subject to small uncertainties. In consequence, absolute cross sections were measured at a fixed energy while cross sections as a function of energy were measured relative to the cross section at this energy.

A. Electron target and cross-section measurement

The electron target for the electron-anion collisions is delivered by the electron cooler [78,79]. The relative electron-ion energy is determined from

$$E=\tfrac{1}{2}m(\nu_i-\nu_e)^2=\left[\left(\frac{m}{M_i}E_i\right)^{1/2}-\sqrt{E_e^{\mathrm{LAB}}}\right]^2, \qquad (11)$$

where M_i is the ion mass and E_i is the ion energy. The relative energy is negative if $\nu_e<\nu_i$ and positive otherwise. Since $M_i \gg m$, the distribution of relative velocities is mainly determined by the electron velocity distribution, $f(\nu)$, and we consider the rate coefficient:

$$\langle \nu\sigma\rangle=\int \nu\sigma(\nu)f(\boldsymbol{\nu})d\boldsymbol{\nu}, \qquad (12)$$

which is the velocity-weighted cross section. The electron velocity distribution in the rest frame of the ions is modeled by a flattened Maxwellian function centered on the detuning velocity $\Delta=|\boldsymbol{\nu}_i-\boldsymbol{\nu}_e|$ between ions and electrons [78], where $\boldsymbol{\nu}_i$ is the ion velocity:

$$f(\boldsymbol{\nu})=\frac{m}{2\pi kT_\perp}e^{-m\nu_\perp^2/2kT_\perp}\left(\frac{m}{2\pi kT_\parallel}\right)^{1/2}e^{-m(\nu_\parallel-\Delta)^2/2kT_\parallel}, \qquad (13)$$

where $\nu_\perp$ and $\nu_\parallel$ are the electron velocity components perpendicular and parallel to the ion beam velocity direction in the rest frame of the ions [the relative energy is $E=\frac{1}{2}m(\nu_\perp^2+\nu_\parallel^2)$]. The longitudinal temperature ($kT_\parallel$) is small because of the compression of the longitudinal electron velocity distribution due to the acceleration of the electrons and $kT_\parallel \sim 0.5$–1.0 meV [78]. The cross area of the electron beam was adiabatically expanded [81] a factor of 6 in a decreasing magnetic field from the gun to the interaction region and the expected transverse temperature was $kT_\perp \sim 20$ meV.

The distribution in relative energy is well approximated by a Gaussian distribution of width $\delta E=\frac{1}{2}kT_\parallel+kT_\perp+(2kT_\parallel E_0)^{1/2}$, where $E_0=\frac{1}{2}m\Delta^2$ is the detuning energy. It is seen that the transverse temperature determines the energy resolution at low energies (<1 eV) while at higher energies the longitudinal temperature is the more important. Above the threshold for detachment of all investigated systems $E>kT_\perp$, and the cross section is to a good approximation given by $\sigma=\langle\nu\sigma\rangle/\Delta$.

Experimentally, the rate coefficient for a process leading to a particle of type X is determined as

$$\langle \nu\sigma\rangle=\frac{R(X)-R_0(X)f_l}{R(AB^-)}\frac{\nu_i}{L_0\epsilon_d\rho_e}, \qquad (14)$$

where $R(X)$ is the measured rate of particles when the electron beam is switched on, $R_0(X)$ is the corresponding rate when the electron beam is switched off, $R(AB^-)$ is the rate of ions entering the interaction region, L_0 ($=85$ cm) is the length of the interaction region, ϵ_d ($=1$) is the detector efficiency, and ρ_e is the electron density. The factor $f_l=\exp(-T_{\mathrm{ch}}/\tau)$, where $1/T_{\mathrm{ch}}$ is the chopping frequency and τ the storage lifetime corrects for the effect that $R(X)$ is measured a little later than $R_0(X)$ by the the chopping technique.

In the toroid regions where the electron beam bends to merge and separate from the ion beam, the two beams are not strictly parallel. The contributions from the toroid regions are subtracted from the measured cross sections by an iterative analysis procedure.

B. Separation of detachment and detachment plus dissociation

The surface barrier detectors measure the energy deposited in the silicon material during the stopping of the incoming particles. Detachment events (AB^0) and detachment plus dissociation events (A^0+B^0) cannot be distinguished on the detector since these events deposit the same amount of energy. To surpass this problem, we used a method where a grid of known transmission, T, was inserted in front of the detector. Particles stopped by the grid will not contribute to the energy deposit and intensity will be transferred from a peak at the full energy (A^0+B^0) to peaks of fractional energies (A^0 or B^0). The technique using grids to distinguish dissociating and nondissociating events has previously been used in a variety of studies [82–90].

For the grid technique to work, the fragments from dissociation must arrive at the detector within a time shorter than the response time of the detector ($\sim\mu$sec) and the particles must be separated by more than the hole diameter (55 μm) [91] when impinging on the grid. For a diatomic molecule dissociating into neutral atomic fragments in the electron cooler with an angle θ between the center-of-mass velocity and the direction of dissociation, the temporal (Δt) and spatial separation (Δr) of the fragments when arriving at the grid/detector are given by

$$\Delta t = L\left(\frac{m_A+m_B}{2E_0}\right)^{1/2}\left(\frac{\Delta E}{E_0}\right)^{1/2}\frac{m_A+m_M}{\sqrt{m_A m_B}}\cos\theta,$$
$$\Delta r = L\left(\frac{\Delta E}{E_0}\right)^{1/2}\frac{m_A+m_B}{\sqrt{m_A m_B}}\sin\theta, \quad \Delta E \ll E_0, \tag{15}$$

where L is the distance from the dissociation point to the grid/detector, ΔE is the energy available for dissociation in the rest frame of molecules, E_0 is the center-of-mass energy in the laboratory frame, and m_A and m_B are the atomic masses. In the present experiment the release energies are of the order of a few eV. For the beams investigated here (see Table I), it is seen that the maximum (at $\theta=0°$) temporal separation between fragments will typically be a few nsec. For the maximum spatial separation to match the hole diameter, an energy of only $\sim$100 μeV has to be available for dissociation. For isotropic dissociation in the center-of-mass system, the corresponding spatial distribution at the grid position is strongly peaked at the maximum separation. Thus, the grid method is applicable to our studies.

To illustrate the effect of the grid, Fig. 2 shows the energy spectra obtained from the surface barrier detector with ($T=71\%$) and without ($T=100\%$) the grid in front of the detector for a 4.8-MeV BN^- beam. Neutrals are produced due to collisions with the residual gas in the ring. The intensity transfer from the higher to the lower peak is clearly seen when the two spectra are compared. The data in Fig. 2 are consistent with a branching ratio of final products BN, B+N, and B or N of $\sigma_{BN}:\sigma_{B+N}:(\sigma_B+\sigma_N)=0.58:0.12:0.30$ for collisions in the residual gas.

In the actual measurement, the rate of the fractional (R_1) and the full (R_2) energy peaks is related to the cross section for detachment (σ_{AB}), detachment plus dissociation (σ_{A+B}), and dissociation leading to one neutral fragment (σ_A or σ_B) in the following way:

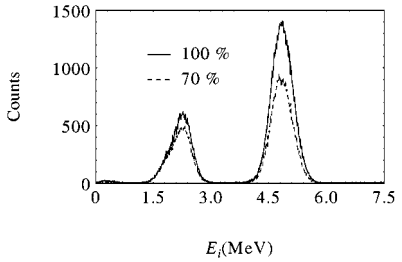

FIG. 2. Energy spectra obtained from the neutral particle surface barrier detector with ($T=71\%$) and without ($T=100\%$) the grid in the front of the detector for a stored 4.8-MeV BN^- beam. Neutrals are here produced by collisions with the residual gas. The high-energy peak at 4.8 MeV is due to impact of BN^0 or B^0 and N^0; the low-energy peak is due to impact of either B^0 or N^0 (which are not resolved).

$$R_1(T)=\frac{1}{N(T)}[T(\sigma_A+\sigma_B)+2T(1-T)(\sigma_{A+B})],$$
$$R_2(T)=\frac{1}{N(T)}[T\sigma_{AB}+T^2\sigma_{A+B}], \tag{16}$$

where $N(T)$ is a normalization factor. These equations are solved to yield the individual cross sections.

C. Charged-particle detection

The negatively charged fragments (X^-) from dissociative reactions of the homonuclear molecules ($e^-+X_2^-\rightarrow X^-+X^-/X^-+X^0+e^-/X^-+X^++2e^-$) are detected with the horizontally movable surface barrier detector positioned inside the dipole magnet following the electron cooler (see Fig. 1). The detector size is relatively small (20 mm diam) to fit into the magnet gap. We investigated whether detection of charged fragments is possible by calculating the spatial distribution of charged particles at the position of the detector and comparing with the measured profile. To determine the distribution of charged fragments (X^-) from a dissociative reaction in the electron cooler, knowledge is required about (i) the distribution of the stored ions inside the electron cooler, (ii) the energy available for dissociation and the angular distribution of dissociations fragments, and (iii) the path of the X^- particles in the magnetic lattice of the storage ring from the electron cooler to the detector.

The evolution of the spatial distribution of a stored ion beam is governed by the magnetic lattice of the storage ring. The propagation of the beam particles can be described using the principles of geometrical optics (the paraxial approximation) [92]. This description is used to calculate the phase-space profile of a stored ion beam at all places in the ring. Similarly, the propagation of X^- particles from the electron cooler to the detector is computed by means of this formalism [93]. We have performed Monte Carlo simulations of the spatial distributions at the detector position of B^- particles emerging from a stored 4.8-MeV beam of B_2^- dissociating in the electron cooler with various release energies. The dissociation was assumed to be isotropic in the center-of-mass frame of the molecular ion. The analysis showed as an important result that the distribution of B^- at the detector po-

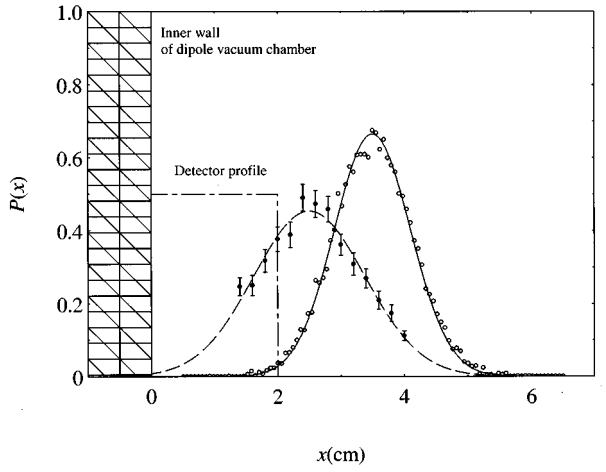

FIG. 3. Distribution $P(x)$ of B^- particles at the position of the movable detector emerging from a stored 4.8-MeV B_2^- beam dissociating in the electron cooler as a function of the horizontal position (x) in the magnet. The dot-dashed line shows the detector profile at horizontal position $x=0$. The filled points show the measured beam profile for a relative electron energy of 5 eV. The dashed line is a Gaussian fit to the measured profile and the full curve is a deconvolution of this function by the detector profile. The open points show the results of the Monte Carlo simulation of the B^- distribution.

sition is independent of the release energy, at least for release energies <20 eV. Figure 3 shows the measured B^- particle intensity profile as a function of the horizontal position of the movable detector for an electron energy $E=5$ eV in comparison with a calculated intensity profile. The measured profile has been fitted with a Gaussian function and this function has been deconvoluted with the detector profile by inverse Fourier transform [94] to compare with the calculated profile. The agreement between the deconvoluted and calculated intensity profiles is excellent and $\sim$80% of the particles can be detected with the 20-mm-diam detector. In conclusion, charged fragments from dissociative reactions leading to an X^- particle in the final state can be detected reliably with the movable 20-mm-diam surface barrier detector when the 20% loss is taken into account.

IV. *AB INITIO* CALCULATIONS

We have performed *ab initio* calculations with the GAUSSIAN94 program package [95] on the ground and the excited electronic states of B_2^q, C_2^q, O_2^q, and BN^q, where $q=0,-1,-2$ to support the interpretation of the experimental results. Especially the possible existence of metastable dianions is investigated. The dynamical aspects, for instance the coupling between discrete states of dianions and the various continua accessible to these, are beyond the scope of our calculations.

In *ab initio* calculations both the theoretical model and the basis set chosen are important for an accurate description. The multireference–configuration interaction method (MR-CI) is presently believed to be the best basis-set method over a significant part of the potential-energy surface (see Ref. [96] for a description and further references). Inclusion of correlation in the theoretical model is very important for small anionic systems. In GAUSSIAN94, correlation may be included using various models, such as configuration interaction or quadratic configuration interaction theory [97] (CI or QCI), Møller-Plesset many-body perturbation theory of order $n<6$ (MPn) [98], density-functional theory (DFI), or coupled-cluster theory [99] (CC). QCI and CC methods are preferred to MPn, since electron correlation is described on a higher level with these methods than in the first orders of MPn ($n<5$). The applicability of DFT in describing anions was addressed by Tschumper and Schaefer [100], who found that DFT significantly overestimates electron affinities. QCI and CC methods have been compared in a number of calculations. Watts *et al.* [101] showed that QCI methods are more sensitive to the applied basis set than CC methods in calculations on the BeO molecule. Lee *et al.* [102] found CC theory to be valid for a series of molecular systems even when nondynamical correlation is important, i.e., when the system has multireference character. In a direct comparison between CC and QCI methods applied to study CuF and CuH, Hrusak *et al.* [103] found CC to be superior to QCI. The main problem with using QCI methods is that single excitations are not described accurately compared to CC methods. CC theory includes excitations of the independent-particle model wave function in a multiplicative manner [97,104], whereas QCI (and other CI and MPn methods) do this additively [97]. Thus, there seem to be no cases where it is of advantage to use QCI methods compared to CC methods.

Inclusion of diffuse functions in the basis set provides a more accurate description of the electron density far away from the nuclei, and by including polarization functions the single-particle orbitals are allowed to change shape. We find that both polarization functions and diffuse functions are important for a good description of the molecular geometry and energy separations, an observation consistent with many other studies, e.g., the study of CN^- by Zhan and Iwata [105], where diffuse functions were seen to be essential in accounting for vertical electron detachment energies while polarization functions were seen to be important for a correct description of geometry and vibrational frequencies.

We used a coupled-cluster method with inclusion of single and double excitations and perturbative inclusion of triple excitations, CCSD(T), of a single reference independent-particle wave function (HF) and a contracted Gaussian basis set that includes diffuse and d polarization functions, $6-311+G(d)$. In total, this basis set includes 44 Gaussian basis functions composed of 70 Gaussian primitives. Excited states of other symmetries than the ground state were calculated on the same level of theory by imposing excitations to the initial independent particle configuration. The dissociation limits were determined by summing up the calculated energies of the separate atoms.

In Table II, our calculations of neutral and monoanionic systems are compared with experiments and high-level *ab initio* calculations. For most systems the calculations can be compared to experimental results [106,107,113–115]. The present calculations generally overestimate equilibrium distances by $\leqslant$0.02 Å, dissociation energies are underestimated by 0.4–0.7 eV, and electron affinities are underestimated by $\leqslant$0.5 eV, while the high-level calculations are in closer agreement with experiment. Bruna and Wright [108] per-

TABLE II. A Comparison of *ab initio* calculation from this work with previous calculations and experiments on total energy (E), equilibrium internuclear distance (r_e), vibrational frequency (ω_e), dissociation energy (D_e), and electron affinity (EA) for neutral and monoanionic molecules. Details on the quoted calculations can be found in the references.

		E (a.u.)	r_e (Å)	ω_e (cm^{-})	D_e (eV)	T_e (eV)	EA (eV)	Ref.
$B_2^{0}\ ^3\Sigma_g^-$								
	MRD-CI/basis I	−49.2889	1.59	1025	2.754		1.80[b]	[108]
	CCSD(T)/6−311+$G(d)$	−49.27957	1.61	1024	2.58		1.77	This work
	Experiment		1.59	1051.3	3.1			[107]
$B_2^{-}\ ^4\Sigma_g^-$								
	MRD-CI/basis I	−49.3549	1.6304	1010	4.21[a]	0		[108]
	CCSD(T)/6−311+$G(d)$	−49.34456	1.6438	995	4.36			This work
$^2\Pi_u$	MRD-CI/basis I		1.5637	1097	3.58	0.63		[108]
	CCSD(T)/6−311+$GD(d)$	−49.32233	1.5818	1066	3.75	0.61		This work
$C_2^{0}\ ^1\Sigma_g^+$								
	MR-CI/[5s4p3d2 f1g]		1.248	1803	6.22			[109]
	CCSI (T)/PVQZ	−75.855232	1.242	1864	6.29		3.09	[110]
	CCSD(T)/6−311+$G(d)$	−75.74787	1.2589	1819	5.78		2.92	This work
	Experiment		1.243	1855	6.32		3.27	[107]
$C_2^{-}\ ^2\Sigma_g^+$								
	CCSD(T)/PVQZ	−75.968855	1.267	1799	8.42			[110]
	CCSD(T)/6−311+$G(d)$	−75.85529	1.2847	1772	7.73			This work
	Experiment		1.268	1781.2	8.45			[106]
$O_2^{0}\ ^3\Sigma_g^-$								
	MR-CI/[5s4p(3+1)d2 f1g+(sp)]		1.21	1558	5.065			[111]
	CCSD(T)/6−311+$G(d)$	−150.0449	1.2114	1599	4.58		0.03	This work
	Experiment		1.208	1580	5.214		0.39	[112–115]
$O_2^{-}\ ^g\Pi_2$								
	CCSD(T)/6−311+$G(d)$	−150.046	1.354	1128	3.7			This work
	Experiment		1.347	1073				[113]
			1.341	1089	4.23			[114]
$BN^{0}\ ^1\Sigma^+$								
	MRD-CI/6s5p3d1f		1.283	1660	6.9		3.13	[116]
	CCSD(T)/6−311+$G(d)$	−79.2299	1.277	1691	6.32[c]		2.82	This work
	Experiment		1.281	1712				
$BN^{-}\ ^2\Sigma^+$								
	MRD-CI/6s5p3d1f		1.291	1709	7.12			[116]
	CCSD(I)/6−311+$G(d)$	−79.33365	1.289	1694	6.76			This work

[a]The electron affinity is given as the energetic differences between the minimum of the neutral and anion potential-energy curves i.e., the difference in zero point vibrational energy is ignored.

[b]The recommended values for B_2^- are $EA(B_2^0)=2.00$ eV and $D_e(B_2^-)=4.80$ eV [108].

[c]We find the $^1\Sigma^+$ state to be 3.93 eV below the ground-state dissociation limit $B(^2P)+N(^4S)$; however, the state is expected to correlate with $B(^2P)+N(^2D)$ [117]. The excited-state limit is positioned 2.389 eV above the ground-state limit [118].

formed *ab initio* calculations on the ground and several excited electronic states of B_2^q ($q=0,-1$) using the multi reference single and double configuration interaction (MRD-CI) method and different basis sets. Eight bound states of B_2^- were reported, the ground state being $^4\Sigma_g^-$ and the lowest doublet being of $^2\Pi_u$ symmetry. Our calculation compares well with these calculations with respect to energies and geometry. BN^q ($q=0,-1$) have been studied by many authors; see Refs. [116,117] for an overview. The present calculation agrees well with a recent MRD-CI study by Bruna *et al.* [116].

Overall, the calculations on neutral and single negatively charged systems compare reasonably well with experiment and other *ab initio* calculations. The underestimation of the dissociation energy is also seen in other studies and probably arises from the assumption that the dissociation limit can be found by summing up the free atom energies. The overestimation of the equilibrium internuclear distances is presumably a basis-set effect as seen by comparing the present calculation with the expanded basis-set calculation of Watts and Barlett [110] for C_2^-. Also the systematic underestimation of electron affinities is seen in other calculations [108].

TABLE III. Comparison of *ab initio* calculation from this work with previous calculations on equilibrium internuclear distance (r_e), vibrational frequency (ω_e), and energy with respect to the monoanionic system [$\Delta E = E(X_2^-) - E(X_2^{2-})$] for the ground states of the studied dianions.

		r_e (Å)	ω_e (cm^{-1})	ΔE (eV)	Ref.
B_2^{2-} $^1\Sigma_g^+$					
	CCSD(T)/6−311+$G(d)$	1.58	1059	−4.0	This work
C_2^{2-} $^1\Sigma_g^+$					
	HF/4-31G	1.271			[52]
	RHF/4-31G	1.271			[56]
	LCAO-MO-SCF/double ζ	1.297			[57]
	HF/6-31G*	1.263	1998		[57]
	MP2/6-31G*	1.30	1716		[57]
	MP2/6-31+$G(d)$	1.293	1737	−2.96	[51]
	see Ref. [59]			−3.0	[59]
	CCSD(T)/6−311+$G(d)$	1.29	1717	−3.9	This work
O_2^{2-} $^1\Sigma_g^+$					
	FSGO	1.490		−16.9	[61]
	SD-CI	1.64	615	−6.68	[64]
	CCSD(T)/6−311+$G(d)$	1.62	507	−7.22	This work
BN^{2-} $^1\Sigma_g^+$					
	HE/4-31G	1.304			[52]
	HF/6-31G*	1.291	1781		[53]
	MP2/6-31+G*	1.325	1528	−2.93	[51]
	MRD-CI/basis A'	1.30	1752	−4.5±0.2	[55]
	CCSD(T)/6−311+$G(d)$	1.31	1585	−3.8	This work

The present calculations of the ground states of dianions are compared to previous studies of dianions in Table III. The $^1\Sigma_g^+$ closed-shell ground state of C_2^{2-} has been considered in many approximations [51,56–59,73]. In the most recent study, this state was described by Sommerfeld *et al.* [59] using a complex absorbing potential together with a multireference configuration interaction wave function. A resonance position of ~3 eV above the ground state of C_2^- and a width of ~0.5 eV towards single electron detachment were reported and a schematic potential energy curve was drawn. The exact position of the resonance was not definitively determined and may possibly vary from 2.8 to 4.0 eV. The present calculation predicts the ground state of C_2^{2-} to be ~3.8 eV above the ground state of C_2^-. Potential-energy curves for the ground state and one excited $^3\Sigma_g$ state of C_2^{2-} were presented by Mathur *et al.* [73] using a method similar to the present one. The present calculation agrees on the ground-state calculation but finds the excited state to be of $^3\Pi_u$ symmetry rather than $^3\Sigma_g$ symmetry [119]. Also for O_2^{2-}, many calculations exist for the closed-shell ground state [60–64]. A high-level potential-energy curve computed with the symmetry-adapted cluster configuration interaction method (SA-CI) for O_2^{2-} ($^1\Sigma_g^+$) was presented by Nakatsuji and Nakai [64], who found the dianion to be energetically 6.68 eV above the ground state of O_2^- with a local potential-energy minimum at 1.64 Å. The present calculation predicts the ground state of O_2^{2-} to be 7.2 eV above the O_2^- ground state and to have an equilibrium distance of 1.62 Å. The ground state of BN^{2-} has been considered on various levels of theory [51–49]. The stability of the ground state of BN^{2-} was described in detail by Bruna *et al.* [55]. As seen from Table III, the present calculation is in good agreement with this high-level study.

In general, the dianion calculations presented here agree with previous calculations for the ground states of BN^{2-}, C_2^{2-}, and O_2^{2-} on both geometrical and energetic aspects. The calculations are expected to be accurate within 0.5–1.0 eV for the relative energy around the equilibrium geometry. Potential-energy curves from the calculations will be presented along with the experimental results in Sec. V.

V. RESULTS

A. B_2^-

The upper part of Fig. 4 shows the cross sections for detachment and detachment plus dissociation obtained with B_2^-. Both the cross section for detachment and for detachment plus dissociation exhibit a smooth behavior as a function of energy. Pure detachment, which is the dominating process, has an effective threshold $E_{\rm th}^{\rm expt}$~3.5 eV and a maximum cross section of 1.2×10^{-15} cm^2 around 16 eV, while the detachment plus dissociation channel has an onset near 4.5 eV and reaches a plateau of 0.3×10^{-15} cm^2 at E ~15–20 eV. The lower part of Fig. 4 shows the cross section for dissociation that leads to detection of B^-. Collisions with the residual gas in the ring contribute little to this channel and it is readily detected even though it is two orders of magnitude smaller than the detachment channel. The disso-

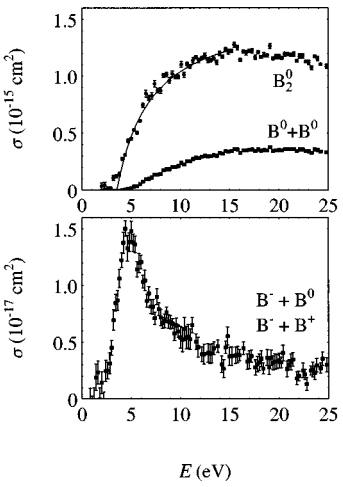

FIG. 4. The cross sections obtained with B_2^- for detachment, detachment plus dissociation, and dissociation as a function of electron energy. In the upper part of the figure, the full curve shows a reaction cross section, $\sigma=\sigma_0(1-E_{\rm th}^{\rm expt}/E)$, with $E_{\rm th}^{\rm expt}=3.5$ eV. The error bars show relative uncertainties; the absolute detachment cross section was measured at $E=15$ eV to be a cross section of $(1.2\pm0.8)\times10^{-15}$ cm^2.

ciation cross section has an onset near 2.1 eV and shows a pronounced peak structure centered around 5 eV with a width of 3–4 eV.

For the ground $^4\Sigma_g^-$ state of B_2^-, the energetic threshold for dissociation is expected around 4.8 eV [108]. The reason for the lower threshold observed in the experiment may be twofold. First, the ions may be rovibrationally excited from the ion source. The rovibrational excitation does not relax by radiative emission since the dipole moment is zero for homonuclear diatomic molecules and the vibrational lifetimes may exceed seconds. Second, other electronic states of B_2^- may be present in the ion beam. Bruna *et al.* [108] predicted three quartet and five doublet states of B_2^- bound with respect to the ground state of the neutral molecule. Only the lifetimes for optical decays from the highest bound quartet state were considered; however, the higher states were predicted to be strongly intercoupled and hence decay to the lowest quartet or doublet state by optical electronic transitions will effectively be allowed. However, the lowest doublet state, $^2\Pi_u$, which is positioned $\sim$ 0.6 eV above the ground $^4\Sigma_g^-$ state (see Table II), can only decay by a forbidden transition and the lifetime of this state may exceed the time scale of this experiment ($\sim$ 5 sec).

The peak structure in the dissociation channel is attributed to the process leading to B^-+B^0 since the energetic threshold for B^-+B^+ is considerably higher, $D_e(B_2^-\,{}^4\Sigma_g^-)+{\rm IP}(B^0)=4.8+8.289=13.089$ eV [108,120]. To investigate the origin of the structure, the results of the *ab initio* calculation on B_2^q ($q=0,-1,-2$) are shown in Fig. 5. The lowest states of B_2^{2-} are of $^1\Pi_u$ and $^1\Sigma_g^+$ symmetry and are $\sim$5 eV above the ground $^3\Sigma_g^-$ state of B_2. There are several excited states of B_2^{2-} in the region where the structure appears in the dissociation cross section. The resonances are all above the dissociation limit of B_2^-. The structure in the dissociation cross section is thus attributed to the formation of a dianion,

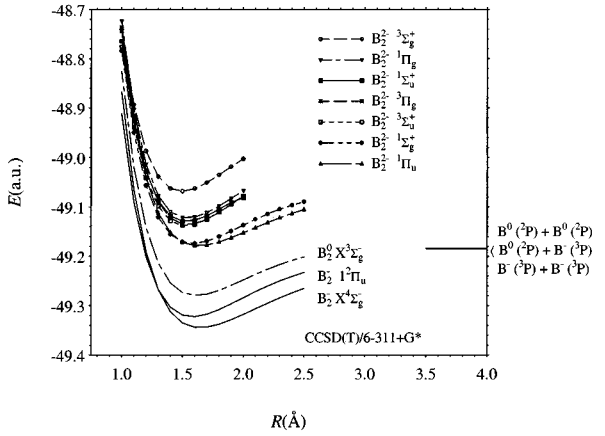

FIG. 5. Potential-energy curves for selected states of B_2^0, B_2^-, and B_2^{2-} obtained on the CCSD(T)/6$-$311$+G(d)$ level of theory.

B_2^{2-}, during the collision process: $e^-+B_2^-\rightarrow\{B_2^{2-}\}\rightarrow B^-+B^0+e^-$. Especially the lowest states of B_2^{2-} exhibit favorable overlap of nuclear wave functions with the ground $^4\Sigma_g^-$ state of B_2^- while the excited states have better overlap with the excited $^2\Pi_u$ state. From the width of the structure, the lifetime of the dianion is $\tau\sim\hbar/\Gamma=(1-2)\times10^{-16}$ sec.

B. C_2^-

The experimental results obtained with C_2^- are shown in Fig. 6. Pure detachment is the dominating process. The detachment cross section has an effective threshold of $\sim$7.0 eV (the electron affinity of C_2 is 3.269 eV [121]) and exhibits a structure near 10 eV. A nonresonant cross section $\sigma=\sigma_0(1-E_{\rm th}^{\rm expt}/E)$ [Eq. (8) or Eq. (10)] has been fitted to the smooth

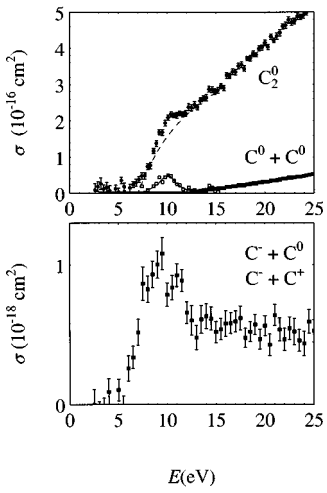

FIG. 6. The cross sections obtained with C_2^- for detachment, detachment plus dissociation, and dissociation as a function of electron energy. In the upper part of the figure, the dashed line shows a reaction cross section, $\sigma=\sigma_0(1-E_{\rm th}^{\rm expt}/E)$, with $E_{\rm th}^{\rm expt}=7.0$ eV. The open squares show the cross section for detachment with the reaction cross section subtracted, and the full curve is a fit to this cross section with $\sigma=\sigma_0/[(E-E_r)^2+\Gamma^2/4]$ ($E_r=10$ eV and $\Gamma=2.1$ eV). The error bars show relative uncertainties; the absolute detachment cross section was measured at $E=13$ eV to be a cross section of $(2.5\pm0.5)\times10^{-16}$ cm^2.

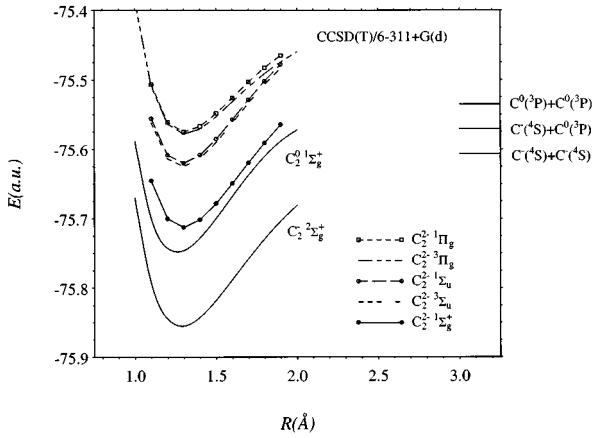

FIG. 7. Potential-energy curves for selected states of C_2^0, C_2^-, and C_2^{2-} obtained on the CCSD(T)/6−311+$G(d)$ level of theory.

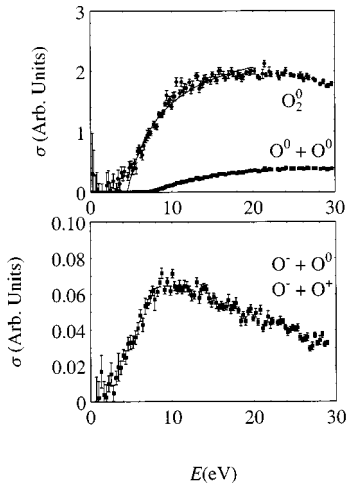

FIG. 8. The cross sections obtained with O_2^- for detachment, detachment plus dissociation, and dissociation as a function of electron energy. In the upper part of the figure, the full curve shows a reaction cross section, $\sigma=\sigma_0(1-E_{\rm th}^{\rm expt}/E)$, with $E_{\rm th}^{\rm expt}=4.5$ eV. The error bars show relative uncertainties.

part of the cross section. The peaklike structure marked by open squares in Fig. 6 shows the cross section when the nonresonant cross section is subtracted. The peak is well fitted with a Lorentzian profile $\sigma=\sigma_0/[(E-E_r)^2+\Gamma^2/4]$ with $E_r=10.0$ eV and $\Gamma=2.1$ eV ($\tau\sim3\times10^{-16}$ sec).

The detachment plus dissociation channel (final C^0+C^0) is characterized by a smoothly rising cross section with a threshold at ~12 eV. For comparison, the energetic threshold is 9.72 eV [122]. No structures are observed in the detachment plus dissociation channel.

In the dissociation cross section (final C^-+C^0), a peak structure is observed at approximately the same energy as the peak in the detachment cross section, i.e., around 10 eV, but with a width of 3–4 eV. The threshold for dissociation from the ground state of C_2^- is $D_0=8.33$ eV [122] while the observed threshold is about 5 eV. The C_2^- ion can be vibrationally excited in the measurement. In particular, the vibrational levels $v>2$ of the ground state of C_2^- decay on a time scale of milliseconds [123,124] due to an interelectronic coupling between the ground $X\ ^2\Sigma_g^+$ and the first excited $A\ ^2\Pi_u$ state of C_2^-, while the lifetime of lower vibrational levels exceeds 5 sec [123]. Since the effective threshold in the cross section for detachment is not lower than expected (see the discussion section), only a small part of the beam is expected to be in higher vibrational states. The fact that the dissociation cross section has a threshold lower than the energetic threshold indicates that the dissociation cross section may have a strong vibrational dependence.

The structures in the cross sections for detachment and dissociation are attributed to the formations of dianions (C_2^{2-}) during the collision process. The different widths of the structures in the cross section for detachment and dissociation could be evidence of different dianionic states being involved in the reactions.

Potential-energy curves for C_2^q ($q=0,-1,-2$) are shown in Fig. 7. The closed-shell $^1\Sigma_g^+$ ground state of C_2^{2-} is positioned around 3.8 eV above the ground state of C_2^- and there are excited states of C_2^{2-} of Σ_u symmetry at ~6.3 eV and of Π_g symmetry at ~7.6 eV. From the present *ab initio* calculation, it is inferred that the structures seen in the detachment and the dissociation cross sections may be due to resonant electron capture into a dianionic state during the collision. However, the dianionic state is probably not the ground state of C_2^{2-}, and hence electronic excitation is involved in the electron-capture process. This is in accord with a theoretical study [59] addressing the structure in the C_2^- detachment cross section, where it was concluded that the structure could not be due to the lowest electronic state of C_2^{2-}. It is an open question which states are involved, but the present calculation demonstrates that excited states of C_2^{2-} exist in the energy range where the structures are observed and the nuclear overlap to those from the ground state of C_2^- is favorable, all states having nearly the same equilibrium internuclear distance.

C. O_2^-

The upper part of Fig. 8 shows the measured cross sections for detachment and detachment plus dissociation, and the lower part shows the cross section for dissociation leading to final O^-. For O_2^-, only relative cross sections were obtained.

The effective threshold for detachment is seen at 4.5 eV and the cross section reaches smoothly a broad plateau around 20 eV, after which a declining tendency is observed. The energetic threshold for detachment is 0.451 eV [113].

The cross section for detachment plus dissociation increases monotonically above the effective threshold at 7.0 eV and over the entire investigated energy range. The energetic threshold for detachment plus dissociation is $D_e(X\ ^2\Pi_g)+EA(O)=4.09+1.46=5.55$ eV [114,125].

The dissociation cross section opens at 2.5 eV and reaches a maximum at 10 eV, after which it decreases approximately as $E^{-1/2}$. The threshold for dissociation from the ground vibrational level is 4.09 eV [114]. Vibrational excitation in the O_2^- beam is not expected to be significant for $v>3$, since higher vibrational states can vibrationally autodetach to the ground state of O_2^0 [126] on a time scale much faster than the time scale of this experiment. In consequence, the low threshold for dissociation is evidence of a strong vibra-

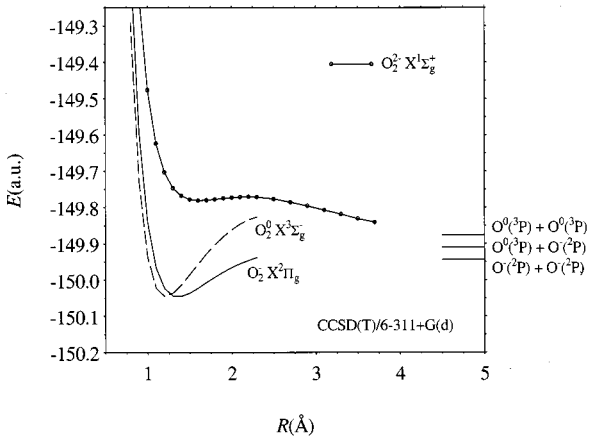

FIG. 9. Potential-energy curves for selected states of O_2^0, O_2^-, and O_2^{2-} obtained on the CCSD(T)/6−311+$G(d)$ level of theory.

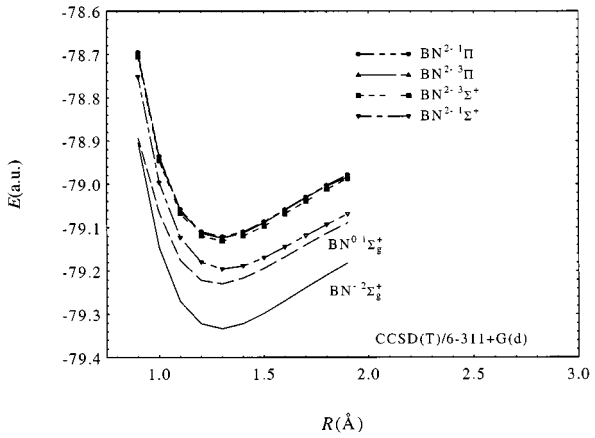

FIG. 11. Potential-energy curves for selected states of BN^0, BN^-, and BN^{2-} obtained on the CCSD(T)/6−311+$G(d)$ level of theory.

tional dependence of this cross section.

Figure 9 shows the calculated potential-energy curves for O_2^0, O_2^-, and O_2^{2-}. The closed-shell $^1\Sigma_g^+$ ground state of O_2^{2-} is positioned 7.2 eV above the ground state of the O_2^{2-}. Two states of Π_u symmetry were identified at higher energies, however they were not bound potential-energy curves. Even though dianionic states are present in the calculations, no evidence of resonances is seen in the cross section either for detachment or for dissociation. The nuclear wave functions of the anion and dianion have poor overlap, and hence a capture reaction from the ground state of the anion would involve electronic to vibrational energy transfer, a process that is probably much weaker than a direct electronic process.

D. BN^-

Figure 10(a) shows the measured cross sections for detachment and detachment plus dissociation. The detachment cross section shows a smooth behavior with an effective threshold at ~ 5.9 eV and a maximum at ~ 27 eV. At energies just above the effective threshold, the energy dependency of the detachment cross section is well represented by $\sigma(E)=\sigma_0(1-E_{\rm th}^{\rm expt}/E)$ [full curve in Fig. 10(b)]. The detachment plus dissociation cross section has an onset around 7.3 eV and increases monotonically over the entire energy range. The energetic threshold for detachment plus dissociation is 7.12 eV [116].

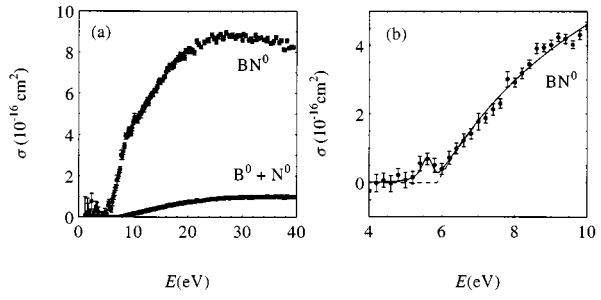

FIG. 10. Experimental cross sections for electron impact detachment of BN^- ($X\ ^2\Sigma^+$). (a) Detachment and detachment plus dissociation cross sections over the full energy range. (b) The detachment cross section near the threshold. The dashed curve is a fit to the threshold region with a reaction model, $\sigma(E)=\sigma_0(1-E_{\rm th}^{\rm expt}/E)$, with $E_{\rm th}^{\rm expt}=5.9$ eV. The solid line shows a superposition of the reaction cross section and a Lorentzian profile, $\sigma=\sigma_0/[(E-E_r)^2+\Gamma^2/4]$ ($E_r=5.6$ eV and $\Gamma=0.4$ eV). The error bars show relative uncertainties; the absolute detachment cross section was measured at $E=11$ eV to be a cross section of $(5.0\pm1.0)\times10^{-16}$ cm^2.

The BN^- beam is not expected to be vibrationally excited. The dipole moment of this anion was calculated to be −1.184 D at $R_e=2.440$ Å [116] and the lifetimes of the first and second excited vibrational levels were calculated to be 154 and 86 msec, respectively, which is much smaller than the elapsed time between ion production and measurement (~5 sec).

The detachment cross section near the effective threshold is shown in Fig. 10(b). At ~5.6 eV, a small peak structure is observed. This structure is well represented by a Lorenzian profile, $\sigma=\sigma_0/[(E-E_r)^2+I^2/4]$, with a peak position $E_r=5.6$ eV and a width of $\Gamma=0.4$ eV. In energy, this structure is close to the position of the closed-shell $^1\Sigma_g^+$ ground state of the BN^{2-} dianion described by Bruna *et al.* [55]. They predicted that a valencelike resonance $^1\Sigma^+(5\sigma^2\pi^4)$ lies 4.5 ± 0.2 eV above the $^2\Sigma^+(5\sigma^2\pi^4)$ ground state of BN^-, and that this state is stable towards dissociation by 2.70 eV. To describe the decay of this resonance, singlet states ($^1\Sigma^+$) originating from electron configurations $5\sigma\pi^4n\sigma$ (shape resonance) and $5\sigma^2\pi^3np_\pi$ (Feshbach resonance) were considered. In Ref. [55], it was concluded that at low energies the resonances autodetach into the BN^-+e^- continuum through mixing with other singlet states of shape resonance character, i.e., $^1\Sigma^+(5\sigma\pi^4n\sigma)$. The influence of triplet states in the decay of $^1\Sigma^+(5\sigma^2\pi^4)$ was not considered by Bruna *et al.* [55].

In Fig. 11, potential-energy curves resulting from the present *ab initio* calculations on BN^0, BN^-, and BN^{2-} are displayed. The ground state of BN^{2-} is positioned ~3.7 eV above the ground state of BN^-, while there are states of Σ and Π symmetry situated at ~5.6 eV. The structure at 5.6 eV in the detachment cross section is attributed to a resonance corresponding to BN^{2-}. The observed width corresponds to

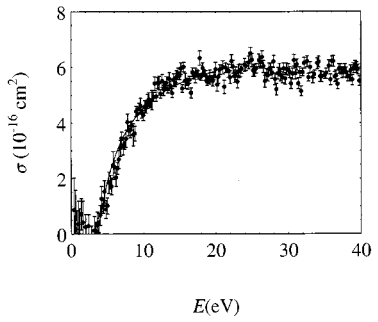

FIG. 12. Total cross section for detachment, detachment plus dissociation, and dissociation leading to a neutral oxygen atom for electron collisions with OH^-. The error bars show relative uncertainties; the absolute cross section was measured at $E=20$ eV to be a cross section of $(6.0\pm2.5)\times10^{-16}$ cm^2.

a resonance lifetime of $\tau\sim\hbar/\Gamma=1.6\times10^{-15}$ sec. Thus, from the present *ab initio* calculations it seems likely that the resonant detachment proceeds through excited states of the dianion and not through the ground state.

E. OH^-

In Fig. 12 the total cross section for detachment, detachment plus dissociation, and dissociation leading to a free O^0 is shown. Only this summed-up cross section is reported because the full energy (E_{OH}) peak and the peak at $16/17E_{OH}$ were not clearly separable in the signal from the surface barrier detector. However, the cross section is dominated by detachment, the O^0 channel being hardly seen in the spectra. The total cross section has an onset at $\sim$3.7 eV and increases until 20 eV, where it reaches a plateau. For comparison, the electron affinity of OH is 1.828 eV [127].

VI. DISCUSSION

A. Detachment

In Fig. 13, the effective threshold observed in detachment is plotted versus the electron binding energy together with results from previous measurements for the atomic ions D^- [13] and O^- [15]. A linear fit for the atomic ions is shown. Disregarding O_2^-, the effective threshold for the molecular

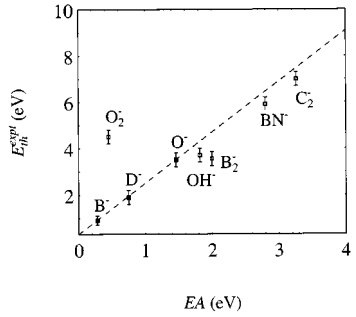

FIG. 13. Effective threshold in detachment cross sections vs the electron affinity. The open squares represent the present measurements on molecular ions while filled squares are taken from previous measurements on atomic ions [13,14]. The dashed line is a linear fit for atomic ions: $E_{th}^{expt}=2.2EA+0.27$ eV.

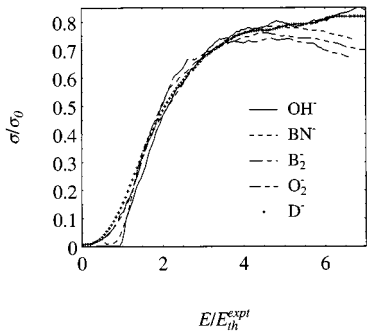

FIG. 14. Comparison of detachment cross section for the studied molecular anions. The energy scale has been normalized to an effective thresholds, E_{th}^{expt}, found by fitting a reaction cross section, $\sigma(E)=\sigma_0(1-E_{th}^{expt}/E)$, to the threshold regions of the cross sections. The cross sections have been normalized to σ_0.

systems mimics the general linear dependence of the electron affinity as seen for atomic ions. As previously discussed, the threshold for B_2^- is lower than expected presumably due to electronic and/or vibrational excitation in the stored ion beams. The molecular thresholds are generally lower than expected from the atomic extrapolation. The reason for this may simply be an effect of the larger spatial extent of the molecular electronic wave functions or that some rovibrational excitation remains in the ion beams. However, it can also be an effect of the cylindrical symmetry in diatomic ions compared to the spherical symmetry for atomic ions. The similarity of the atomic extrapolation and the values for the molecular systems indicates that close to threshold the nonresonant detachment happens through a similar mechanism for both atomic and molecular ions.

The threshold for detachment from O_2^- is significantly higher than expected from the atomic extrapolation and the reason is presumably the fact that the nuclear wave functions of the ground states of the anion and the neutral molecule have an unfavorable overlap [115].

The energy dependence of the detachment cross section for the studied molecular systems is compared in Fig. 14. In the threshold region, the detachment cross sections have been fitted with a reaction cross section $\sigma(E)=\sigma_0(1-E_{th}/E)$ [Eq. (8) or Eq. (10)]. The energy axis has been scaled with the effective threshold for each ion. To facilitate a comparison of the shape of the cross sections, these have been normalized to σ_0 as found from the fit to the threshold region. For comparison, the cross section for detachment from an atomic ion, D^- [13], has been added. The energy dependence of the cross section is very similar for the investigated molecular systems and for the atomic systems. Near threshold, B_2^- and O_2^- have tails reaching below the effective threshold while more steep increases are seen for BN^- and OH^-. Close to threshold, detachment probably takes place by tunneling, which may be sensitive to the actual ion structure. As for the atomic ions, at $E>5E_{th}^{expt}$ the cross sections start to deviate and the detachment process is again dependent on the specific target structure.

The nonresonant detachment process may proceed as either a one- or a two-step process:

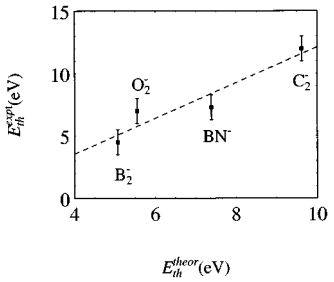

FIG. 15. Experimental thresholds for detachment plus dissociation vs the energetic threshold. The experimental thresholds have been found from fitting a reaction cross section, $\sigma=\sigma_0(1-E_{\rm th}^{\rm expt}/E)$, to the threshold regions and the error bars are estimated from the flexibility of the fitting parameter $E_{\rm th}^{\rm expt}$. The energetic threshold, $E_{\rm th}^{\rm theor}$, has been deduced from experimental data (C_2^- [122] and O_2^- [113,114]) or high-level *ab initio* calculations (B_2^- [108] and BN^- [116]). The dashed line is a linear fit: $E_{\rm th}^{\rm expt}=1.4E_{\rm th}^{\rm theor}-2.2$ eV.

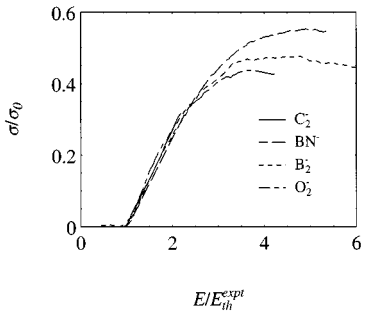

FIG. 16. Comparison of shapes of detachment plus dissociation cross section for the studied molecular anion. The scales have been normalized to $E_{\rm th}^{\rm expt}$ and σ_0 found by fitting, $\sigma(E)=\sigma_0(1-E_{\rm th}^{\rm expt}/E)$, to the threshold regions of the actual cross sections.

$$e^-(E_i)+AB^-(\alpha_i)\rightarrow AB^0(\alpha_f)+e^-(E_1)+e^-(E_2)$$
$$\rightarrow AB^-(\beta)+e^-(E_1)\rightarrow AB^0(\alpha_f)+e^-(E_2), \quad (17)$$

where E_i, E_1, and E_2 are electron kinetic energies, while α_i, α_f and β represent rovibronic states. The two-step process proceeds through a resonance state of the anion. This is, however, not expected to yield pronounced structures in the cross section since the excitation process can happen at any incident electron energy above the excitation energy. The final state of the neutral system, $AB^0(\alpha_f)$, or the intermediate anion state, $AB^-(\beta)$, may eventually be in dissociative continua, thus contributing to detachment plus dissociation or pure dissociation. It is emphasized that the present experiment cannot distinguish these two reaction pathways.

To summarize, the energy scale of the detachment cross section is characterized by the effective threshold, which depends on both the electronic binding energy and the overlap between the nuclear wave functions. The energy dependence of the cross section is similar in the studied systems, but variations are seen near threshold and towards higher energies. The regularity in the effective thresholds and the similar shapes of the cross sections indicate a common mechanism for nonresonant detachment for the studied anions.

B. Detachment plus dissociation

All measured cross sections for detachment plus dissociation exhibit a smoothly rising energy dependence from threshold. Near the threshold, the cross section can be represented by a reaction cross section of the form $\sigma=\sigma_0(1-E_{\rm th}^{\rm expt}/E)$. In Fig. 15, these experimental thresholds for detachment plus dissociation are plotted versus the energy threshold. The experimental points have been fitted with a linear function that reproduces the general tendency. The shapes of the cross sections for detachment plus dissociation are compared in Fig. 16. To facilitate the comparison, the energy and cross-section axes have been scaled by $E_{\rm th}^{\rm expt}$ and σ_0, respectively, which were found by fitting a reaction cross section to the threshold region. For $E<3E_{\rm th}^{\rm expt}$, the cross sections are similar while for higher energies deviations are seen. The similarity of the shapes of the cross section points to similar mechanisms for detachment plus dissociation.

Nonresonant mechanisms for detachment plus dissociation that fulfill these requirements can proceed in various ways. One likely mechanism is a vertical transition to a dissociative potential-energy curve of the neutral molecule, i.e., effectively a two-step process:

$$e^-(E_i)+AB^-(\alpha_i)\rightarrow AB^0(\beta)+e^-(E_1)+e^-(E_2),$$
$$AB^0(\beta)\rightarrow A^0(\alpha_1)+B^0(\alpha_2)+\Delta E_{\rm dis}, \quad (18)$$

where the first step is the fastest. E_i, E_1, and E_2 are electron kinetic energies; α_i, β, α_1, and α_2 represent rovibronic states; and $\Delta E_{\rm dis}$ is the kinetic energy available for dissociation. Alternatively, the process may proceed through an anionic resonance, $AB^-(\beta)$, as in the two-step detachment process, Eq. (17). Even though the process involves a resonance state, $AB^0(\beta)$ or $AB^-(\beta)$, no resonance structures are expected in the cross section since this detachment-excitation reaction may happen for all energies above threshold. The excited state $[AB^0(\beta)]$ can also decay to a bound state of AB^0 by radiative emission and hence contribute to the pure detachment reaction, however radiative lifetimes are typically of the order of nanoseconds while vibrational motion takes place on a time scale of 10^{-14} sec. It is considered unlikely that energy is transferred to the nuclear motion in the initial steps of the reaction since the electronic time scale (10^{-16} sec) is much faster than the nuclear time scale. Finally, the suggested mechanism with a vertical coupling to a dissociative curve is supported by the fact that the observed threshold for detachment plus dissociation is generally higher than the energetic threshold.

C. Dissociation

The measured dissociation cross sections of the homonuclear molecules have thresholds that are lower than the energetic threshold expected from the ground vibronic state of the ions. From the close agreement between the detachment thresholds for molecular and atomic ions, it is inferred that only small parts of the ion beams are vibrationally ex-

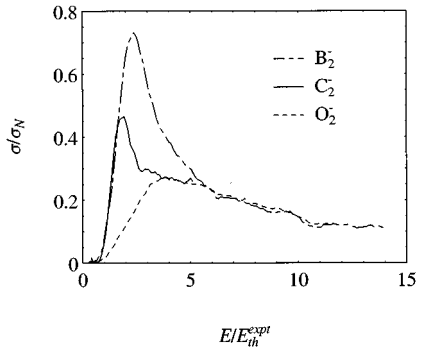

FIG. 17. Comparison of dissociation cross sections (final X^-) for the studied homonuclear molecular systems. The energy scales have been normalized to the experimental threshold, $E_{\rm th}^{\rm expt}$, while the cross sections are scaled to match the same asymptote towards high energy.

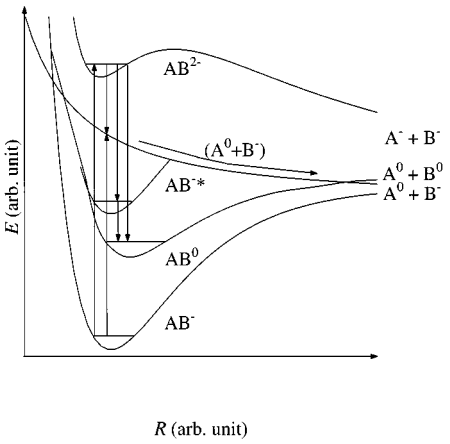

FIG. 18. A schematic drawing of potential-energy curves of a diatomic molecule and its negative ions. The vertical arrows indicate some decays to bound and repulsive curves of the negative and neutral systems.

cited. Hence, the dissociation cross sections must have a strong vibrational dependence with the cross section for higher vibrational levels being the larger. Experiments that could reveal the vibrational dependence of the cross section either through active state manipulation [30,128] or direct probing [30] of the state distribution are highly desirable.

The shapes of the dissociation cross sections are compared in Fig. 17. The energy scales have been normalized to the experimental thresholds and the cross sections have been scaled to match the same asymptote towards higher energies. While the cross sections for B_2^- and C_2^- exhibit significant peaklike structures around $2-3E_{\rm th}^{\rm expt}$, the dissociation cross section for O_2^- has a smooth energy dependence with a maximum at $\sim 4E_{\rm th}^{\rm expt}$. It is worth noting that all cross sections match the same asymptotic behavior, thus the cross sections for B_2^- and C_2^- are essentially of the same form as for O_2^- with a peak structure superimposed, suggesting that B_2^- and C_2^- have an extra (resonant) mechanism of dissociation compared to O_2^-.

The mechanism for nonresonant dissociation is likely to proceed through an excited dissociative state of the negative ion:

$$\begin{aligned} e^-(E_i)+AB^-(\alpha_i)&\rightarrow AB^-(\beta)+e^-(E_1),\\ AB^-(\beta)&\rightarrow A^-(\alpha_1)+B^0(\alpha_2)+\Delta E_{\rm kin}, \end{aligned} \tag{19}$$

since, as was argued for detachment plus dissociation, direct transfer of energy to the nuclear motion is probably less favorable compared to electronic excitation.

D. Metastable dianions

Overall, the measured cross sections are slowly varying functions of energy, except for significant structures in the cross section for detachment of C_2^- and BN^- and dissociation of B_2^- and C_2^-. The structures in the cross sections for detachment and dissociation for C_2^- occur at almost the same energy ($\sim$10 eV) but have different widths ($\sim$2 eV for detachment, 3–4 eV for dissociation). For B_2^- no structure is observed in the detachment channel. The structures in the cross sections are interpreted as the formation of resonances during the collision process and the mechanism is formally written as

$$e^-(\varepsilon_i)+AB^-(\alpha_i)\rightarrow AB^{2-}(\beta)\rightarrow \text{products}. \tag{20}$$

From the widths of the resonances, lifetimes of the order of $\tau\sim\hbar/\Gamma\sim(1-3)\times10^{-16}$ sec are predicted. The performed *ab initio* calculations show that the dianionic states exist in the regions where the structures are observed (see Figs. 5, 7, and 11). For detachment of C_2^- and BN^-, the relevant dianions are excited with respect to the ground dianionic states, while both the ground and excited states of B_2^{2-} may be important for dissociation of B_2^-.

The *ab initio* calculations point to the existence of metastable dianions of B_2^-, C_2^-, O_2^-, and BN^- and the dianions are generally unstable to single detachment (AB^-+e^-), double detachment (AB^0+2e^-), and dissociation ($X^-+X^0+e^-$). In Fig. 18, some typical potential-energy curves for a neutral molecule, AB^0, and its negative ions are shown together with some possible decay mechanisms for a dianionic state. Structures are the exception rather than the rule in the measured cross sections, and in detachment the structures are superimposed on dominating nonresonant backgrounds. Thus, at least two factors are important for the resonant capture process to be effective: (i) the penetration probability through the repulsive Coulomb barrier (plus perhaps an angular momentum barrier) [66–68,129] must be nonvanishing, and (ii) the nuclear wave functions in the initial and final state must have a favorable overlap or the electron-vibrational coupling must be very strong. The first condition is supported by the observation that excited states of the dianion are important in the capture process. The second condition is exemplified in the case of $e^-+O_2^-$ scattering, where no structures were observed although resonances were predicted by *ab initio* calculations. The fact that electronic excitation is essential for resonant electron capture to occur is also seen in electron-cation reactions, for instance in dielectronic recombination of atomic ions [130] or in the direct dissociative recombination of possive ions [131].

VII. CONCLUSION

The cross sections for detachment, detachment plus dissociation, and pure dissociation by electron impact for the diatomic anions B_2^-, C_2^-, O_2^-, BN^-, and OH^- have been measured for energies below 40 eV at the ASTRID heavy ion storage ring. The dominating reaction for all investigated systems is detachment (final AB^0+2e^-). A significant character of the cross section for detachment is the effective threshold. This depends on the electronic binding energy and the overlap of the nuclear wave functions in the initial and final states and defines an energy scale for the process. The energy dependence of the cross section is similar in the studied systems, however variations are seen near threshold and towards higher energies. The regularity in the effective threshold as a function of electron binding energy and the similar shape of the cross sections indicate a common mechanism for nonresonant detachment for the studied anions. The detachment reaction may proceed either by direct detachment in a one-step process or by sequential detachment through an excited anionic state in a two-step process.

In the process of detachment plus dissociation (final $A^0+B^0+2e^-$), a threshold of a few eV in excess of the energetic threshold is generally observed, however no clear regularity between the experimental and theoretical threshold is seen. The shapes of the cross sections are similar over a wide energy range. Thus, common mechanisms for detachment plus dissociation seem to be evident in the studied systems. The process is likely to proceed through a vertical transition to a dissociative potential-energy curve of the anionic or neutral molecular system.

For homonuclear ions, the cross sections for dissociative reactions (final $A^-+A^0+e^-$) indicate a strong vibrational dependence. The nonresonant part of the measured dissociation cross sections shows a similar decreasing behavior towards high energy, and nonresonant dissociation is likely to proceed through excitation to a dissociative potential-energy curve of the anion.

The formation and decay of diatomic dianions by electron bombardment are addressed. Evidence for metastable dianions with lifetimes of the order of 10^{-16} sec as intermediate collision complexes is found in the cross section for detachment of C_2^- and BN^- and in the cross section for dissociation of B_2^- and O_2^-. The assignment is supported by *ab initio* calculations and it is inferred that electronic excitation is important in the resonant reactions.

More work in both theory and experiment on these processes is desirable. Theoretical work on the electron-anion scattering process is needed to clarify the actual mechanisms underlying the various nonresonant processes. Concerning the formation of dianions, a scattering calculation would probably clarify the important dianionic states and the actual dynamics governing the formation and decay of these. Experimental techniques that can reveal the detailed dynamics of the reaction, for instance by measuring cross sections for selected vibrational levels or energies and angular distributions of the reaction fragments, are desirable.

ACKNOWLEDGMENTS

This work has been supported by the Danish National Research Foundation through the Aarhus Center for Atomic Physics (ACAP). We thank the ASTRID staff for support during the measurements. Jørgen S. Nielsen is acknowledged for providing the charged-particle propagation analysis. One of us (N.D.) was supported in part by the U.S. Department of Energy under Contract No. DE-A102-95ER54293 with the National Institute of Standards and Technology.

[1] G. C. Tisone and L. M. Branscomb, Phys. Rev. Lett. **17**, 236 (1966).
[2] G. C. Tisone and L. M. Branscomb, Phys. Rev. **170**, 169 (1968).
[3] D. F. Dance, M. F. A. Harrison, and R. D. Rundel, Proc. R. Soc. London, Ser. A **299**, 525 (1967).
[4] B. Peart, D. S. Walton, and K. T. Dolder, J. Phys. B **3**, 1346 (1970).
[5] D. S. Walton, B. Peart, and K. T. Dolder, J. Phys. B **4**, 1343 (1971).
[6] B. Peart and K. T. Dolder, J. Phys. B **6**, 1497 (1973).
[7] B. Peart, R. A. Forrest, and K. T. Dolder, J. Phys. B **12**, 847 (1979).
[8] B. Peart, R. A. Forrest, and K. T. Dolder, J. Phys. B **16**, 2735 (1979).
[9] B. Peart, R. A. Forrest, and K. T. Dolder, J. Phys. B **12**, 847 (1979).
[10] B. Peart, R. A. Forrest, and K. T. Dolder, J. Phys. B **16**, 2735 (1979).
[11] B. Peart, R. A. Forrest, and K. T. Dolder, J. Phys. B **12**, L115 (1979).
[12] T. Tanabe, I. Katayama, H. Kamegaya, K. Chida, Y. Arakaki, M. Yoshizawa, Y. Harruyama, M. Saito, T. Honma, K. Hosono, K. Hatanaka, F. J. Currell, and K. Noda, Phys. Rev. A **54**, 4069 (1996).
[13] L. H. Andersen, D. Mathur, H. T. Schmidt, and L. Vejby-Christensen, Phys. Rev. Lett. **74**, 892 (1995).
[14] L. H. Andersen, N. Djuric, M. J. Jensen, H. B. Pedersen, and L. Vejby-Christensen, Phys. Rev. A **58**, 2819 (1998).
[15] L. Vejby-Christensen, D. Kella, D. Mathur, H. B. Pedersen, H. T. Schmidt, and L. H. Andersen, Phys. Rev. A **53**, 2371 (1996).
[16] L. H. Andersen, P. Hvelplund, D. Kella, P. H. Mokler, H. B. Pedersen, H. T. Schmidt, and L. Vejby-Christensen, J. Phys. B **29**, L643 (1996).
[17] H. B. Pedersen, N. Djurić, M. J. Jensen, D. Kella, C. P. Safvan, H. T. Schmidt, L. Vejby-Christensen, and L. H. Andersen, Phys. Rev. Lett. **81**, 5302 (1998).
[18] R. W. Hart, E. P. Gray, and W. H. Guier, Phys. Rev. **108**, 1512 (1957).
[19] E. A. Solov'ev, Zh. Eksp. Teor. Fiz. **72** 2072 (1977) [Sov. Phys. JETP **45**, 1089 (1977)].
[20] B. M. Smirnov and M. I. Chibisov, Zh. Eksp. Teor. Fiz. **49** 841 (1966) [Sov. Phys. JETP **22**, 585 (1966)].
[21] V. N. Ostrovsky and K. Taulbjerg, J. Phys. B **29**, 2573 (1996).

[22] A. K. Kazansky and K. Taulbjerg, J. Phys. B **29**, 4465 (1996).
[23] J. T. Lin, T. F. Jiang, and C. D. Lin, J. Phys. B **29**, 6175 (1996).
[24] M. S. Pindzola, Phys. Rev. A **54**, 3671 (1996).
[25] F. Robicheaux, Phys. Rev. Lett. **82**, 707 (1999).
[26] See, e.g., W. Domcke, Phys. Rep. **208**, 97 (1991).
[27] See, e.g, L. H. Andersen, P. J. Johnson, D. Kella, H. B. Pedersen, and L. Vejby-Christensen, Phys. Rev. A **55**, 2799 (1997).
[28] J. Kalcher and A. F. Fox, Chem. Rev. **94**, 2291 (1994).
[29] M. K. Scheller, R. N. Compton, and L. S. Cederbaum, Science **270**, 1160 (1995).
[30] Active control of the vibrational populations has been demonstrated for H_2^+ [H. T. Schmidt, L. Vejby-Christensen, H. B. Pedersen, D. Kella, N. Bjerre, and L. H. Andersen, J. Phys. B **29**, 2485 (1996)], and direct probing of vibrational distribution during measurement has been demonstrated for HD^+ [Z. Amitay, A. Baer, M. Dahan, L. Knoll, M. Lange, J. Levin, I. F. Schnieder, D. Schwalm, A. Suzor-Weiner, Z. Vager, R. Wester, A. Wolf, and D. Zaifmann, Science **281**, 75 (1998)].
[31] R. D. Levine and R. B. Berstein, *Molecular Reaction Dynamics* (Oxford University Press, New York, 1974).
[32] See, e.g., F. A. Cotton, G. Wilkinson, and P. L. Gauss, *Basic Inorganic Chemistry*, 2nd ed. (Wiley, New York, 1987).
[33] H. S. Taylor and L. D. Thomas, Phys. Rev. Lett. **28**, 1091 (1971).
[34] L. D. Thomas, J. Phys. B **7**, L97 (1974).
[35] R. Schnitzer and M. Anbar, J. Chem. Phys. **64**, 2466 (1976).
[36] F. Robicheaux, R. P. Wood, and C. H. Greene, Phys. Rev. A **49**, 1866 (1994).
[37] B. Simon, Int. J. Quantum Chem. **14**, 529 (1978).
[38] T. Sommerfeld, U. V. Riss, H.-D. Meyer, and L. S. Cederbaum, Phys. Rev. Lett. **77**, 470 (1996).
[39] T. Sommerfeld, U. V. Riss, H.-D. Meyer, and L. S. Cederbaum, Phys. Rev. A **55**, 1903 (1997).
[40] T. Morishita, C. D. Lin, and C. G. Bao, Phys. Rev. Lett. **80**, 464 (1998).
[41] K. T. Chung, Phys. Rev. A **58**, 2777 (1998).
[42] D. R. Herrick and F. H. Stillinger, J. Chem. Phys. **62**, 4360 (1975).
[43] J. W. Gadzuk and C. W. Clark, J. Chem. Phys. **91**, 3174 (1989).
[44] S. Huzinaga and A. Hart-Davis, Phys. Rev. A **8**, 1734 (1973).
[45] W. K. Stuckey and R. W. Kiser, Nature (London) **211**, 963 (1966).
[46] I. H. Bauman, E. Heincke, H. J. Kaiser, and K. Bethge, Nucl. Instrum. Methods **95**, 389 (1971).
[47] L. Frees, E. Heinicke, and W. S. Koski, Nucl. Instrum. Methods **159**, 105 (1979).
[48] D. Spence, W. A. Chupka, and C. M. Stevens, Phys. Rev. A **26**, 654 (1982).
[49] K. H. Chang, R. D. McKeown, R. G. Milner, and J. Labrenz, Phys. Rev. A **35**, 3949 (1987).
[50] A. Galindo-Urbarri, H. W. Lee, and K. H. Chang, J. Chem. Phys. **83**, 3685 (1985).
[51] A. I. Boldyrev and J. Simons, J. Chem. Phys. **98**, 4745 (1993).
[52] N. L. Summers and J. Tyrrell, J. Am. Chem. Soc. **99**, 3960 (1977).
[53] P. Pyykkö, Mol. Phys. **67**, 871 (1989).
[54] P. Pyykkö and Y. Zhao, J. Phys. Chem. **94**, 7753 (1990).
[55] P. J. Bruna, R. M. Mawhinney, and F. Grein, J. Phys. B **29**, 2413 (1995).
[56] D. Poppinger and L. Radom, Chem. Phys. **30**, 415 (1978).
[57] A. C. Hopkinson, K. Yates, and I. G. Csizmadia, Theor. Chim. Acta **23**, 369 (1972).
[58] P. Pyykkö, Chem. Phys. Lett. **156**, 337 (1989).
[59] T. Sommerfeld, U. V. Riss, H.-D. Meyer, and L. S. Cederbaum, Phys. Rev. Lett. **79**, 1237 (1997).
[60] G. Chambaud, B. Levy, and P. Millie, Theor. Chim. Acta **48**, 103 (1978).
[61] A. H. Pakiari and J. W. Linnett, Int. J. Quantum Chem. **18**, 661 (1980).
[62] G. Leroy, D. Peeters, and M. Thange, J. Mol. Struct. **123**, 243 (1985).
[63] M. Roch and J. Weber, Chem. Phys. Lett. **115**, 268 (1985).
[64] H. Nakatsuji and H. Nakai, Chem. Phys. Lett. **18**, 339 (1992).
[65] S. N. Schauer, P. Williams, and R. N. Compton, Phys. Rev. Lett. **65**, 625 (1990).
[66] R. L. Hettich, R. N. Compton, and R. H. Ritchie, Phys. Rev. Lett. **67**, 1242 (1991).
[67] C. Yannouleas and U. Landman, Chem. Phys. Lett. **217**, 175 (1994).
[68] C. Jin, R. L. Hettich, R. N. Compton, A. Tuinman, A. Derecskei-Kovacs, D. S. Marynick, and B. I. Dunlab, Phys. Rev. Lett. **73**, 2821 (1994).
[69] M. K. Scheller and L. S. Cederbaum, J. Chem. Phys. **99**, 441 (1993).
[70] M. K. Scheller and L. S. Cederbaum, J. Phys. B **25**, 2257 (1992).
[71] R. Middelton and J. Klein, Nucl. Instrum. Methods Phys. Res. B **123**, 532 (1997).
[72] R. N. Compton, A. Tuinman, C. E. Klots, M. R. Pederson, and D. C. Patton, Phys. Rev. Lett. **78**, 4367 (1997).
[73] D. Mathur, V. R. Bhardwaj, F. A. Rajgara, and C. P. Savfan, Chem. Phys. Lett. **277**, 558 (1997).
[74] L.-S. Wang, C.-F. Ding, X.-B. Wang, and J. B. Nicholas, Phys. Rev. Lett. **81**, 2667 (1998).
[75] X.-B. Wang, C.-F. Ding, and L.-S. Wang, Phys. Rev. Lett. **81**, 3351 (1998).
[76] S. P. Møller, in *Conference Record of the 1991 IEEE Particle Accelerator Conference, San Francisco*, edited by K. Berkner (IEEE, Piscataway, NJ, 1991), p. 2811
[77] P. Tykesson, H. H. Andersen, and J. Heinemeier, IEEE Trans. Nucl. Sci. **23**, 1104 (1976).
[78] L. H. Andersen, J. Bolko, and P. Kvistgaard, Phys. Rev. A **41**, 1293 (1990).
[79] L. Vejby-Christensen, D. Kella, D. Mathur, H. B. Pedersen, H. T. Schmidt, and L. H. Andersen, Phys. Rev. A **53**, 2371 (1996).
[80] F. Abildskov and S. P. Møller, in *Beam Instrumentation*, edited by Alex H. Lumpkin and Catherine E. Eyberger, AIP Conf. Proc. No. 390 (AIP, Woodbury, NY, 1996), p. 536.
[81] H. Danard, Nucl. Instrum. Methods Phys. Res. A **335**, 397 (1993).
[82] T. J. Morgan, K. H. Berkner, and R. V. Pyle, Phys. Rev. Lett. **26**, 602 (1971).
[83] J. W. Stearns, K. H. Berkner, R. V. Pyle, B. P. Briegleb, and M. L. Warren, Phys. Rev. A **4**, 1960 (1971).
[84] J. B. A. Mitchell, J. L. Forand, C. T. Ng, D. P. Levac, R. E.

Mitchell, P. M. Mul, W. Claeys, A. Sen, and J. Wm. McGowan, Phys. Rev. Lett. **51**, 885 (1983).
[85] S. Abraham, D. Nir, and B. Rosner, Phys. Rev. A **29**, 3122 (1984).
[86] O. Haber, I. Ben-Itzhak, I. Gertner, A. Mann, and B. Rosner, J. Phys. B **18**, L201 (1985).
[87] S. Datz, G. Sundström, Ch. Biedermann, L. Broström, H. Danared, S. Mannervik, J. R. Mowat, and M. Larsson, Phys. Rev. Lett. **74**, 896 (1995).
[88] S. Datz, M. Larsson, C. Stromholm, G. Sundström, V. Zengin, H. Danared, A. Källberg, and M. af Ugglas, Phys. Rev. A **52**, 2901 (1995).
[89] L. H. Andersen, O. Heber, D. Kella, H. B. Pedersen, L. Vejby-Christensen, and D. Zaifmann, Phys. Rev. Lett. **77**, 4891 (1996).
[90] L. Vejby-Christensen, L. H. Andersen, O. Heber, D. Kella, H. B. Pedersen, H. T. Schmidt, and D. Zaifmann, Astrophys. J. **483**, 531 (1997).
[91] The hole diameter of the grids was measured with a light microscope.
[92] J. Rossbach and P. Schmüser, CERN Report No. 94-01, p. 17ff.
[93] J. S. Nielsen (private communication).
[94] See, e.g., A. G. Marshall and F. R. Verdun, *Fourier Transforms in NMR, Optical, and Mass Spectroscopy* (Elsevier, Amsterdam, 1990).
[95] GAUSSIAN 94, revision E.1, M. J. Frisch, G. W. Trucks, H. B. Schlegel, P. M. W. Gill, B. G. Johnson, M. A. Robb, J. R. Cheeseman, T. Keith, G. A. Petersson, J. A. Montgomery, K. Raghavachari, M. A. Al-Laham, V. G. Zakrzewski, J. V. Ortiz, J. B. Foresman, J. Cioslowski, B. B. Stefanov, A. Nanayakkara, M. Challacombe, C. Y. Peng, P. Y. Ayala, W. Chen, M. W. Wong, J. L. Andres, E. S. Replogle, R. Gomperts, R. L. Martin, D. J. Fox, J. S. Binkley, D. J. Defrees, J. Baker, J. P. Stewart, M. Head-Gordon, C. Gonzalez, and J. A. Pople, Gaussian, Inc., Pittsburgh, PA, 1995.
[96] H.-J. Werner and P. J. Knowles, Theor. Chim. Acta **78**, 175 (1990).
[97] J. A. Pople, M. Head-Gordon, and K. Raghavachari, J. Chem. Phys. **87**, 5968 (1987).
[98] C. Møller and M. S. Plesset, Phys. Rev. **46**, 618 (1934).
[99] J. Cizek, J. Chem. Phys. **45**, 4256 (1966).
[100] G. S. Tschumper and H. F. Schaefer III, J. Chem. Phys. **107**, 2529 (1997).
[101] J. D. Watts, M. Urban, and R. J. Bartlett, Theor. Chim. Acta **90**, 341 (1995).
[102] T. J. Lee, A. P. Rendell, and P. R. Taylor, J. Phys. Chem. **94**, 5463 (1990).
[103] J. Hrusak, S. Ten-no, and S. Iwata, J. Chem. Phys. **106**, 7185 (1997).
[104] J. Paldus, J. Čížek, and B. Jeziorski, J. Chem. Phys. **90**, 4356 (1989).
[105] C.-G. Zhan and S. Iwata, J. Chem. Phys. **104**, 9058 (1996).
[106] R. D. Mead, U. Hefter, P. A. Schulz, and W. C. Lineberger, J. Chem. Phys. **82**, 1723 (1985).
[107] K. P. Huber and G. Herzberg, *Molecular Structure and Molecular Spectra IV. Constants of Diatomic Molecules* (Van Nostrand Reinhold, New York, 1979).
[108] P. J. Bruna and J. S. Wright, J. Phys. B **23**, 2197 (1990).
[109] C. W. Bauschlicher, Jr. and S. R. Langhoff, J. Chem. Phys. **87**, 2919 (1987).
[110] J. D. Watts and J. Bartlett, J. Chem. Phys. **96**, 6073 (1992).
[111] H. Patridge, C. W. Bauschlicher, Jr., S. R. Langhoff, and P. R. Taylor, J. Chem. Phys. **95**, 8292 (1991).
[112] T. G. Slanger and P. C. Cosby, J. Phys. Chem. **92**, 267 (1988).
[113] M. J. Travers, D. C. Cowles, and G. B. Ellison, Chem. Phys. Lett. **164**, 449 (1989).
[114] R. J. Celotta, R. A. Bennett, J. L. Hall, M. W. Siegel, and J. Levine, Phys. Rev. A **6**, 631 (1972).
[115] P. H. Krupenie, J. Phys. Chem. Ref. Data **1**, 423 (1972).
[116] P. J. Bruna, R. M. Mawhinney, and F. Grein, Int. J. Quantum Chem., Symp. **29**, 455 (1995), and references therein.
[117] For an overview, see. S. P. Karna and F. Grein, Chem. Phys. **98**, 207 (1985).
[118] *Atomic Energy Levels*, edited by C. E. Moore, Natl. Bur. Stand. (U.S.) Circ. No. 467 (U.S. GPO, Washington, DC, 1949), Vol. 1.
[119] The $^3\Sigma_g$ state of C_2^{2-} reported in Ref. [73] has been revisited by the authors and found to be of $^3\Pi_u$ symmetry (private communication).
[120] D. R. Lide, *Handbook of Chemistry and Physics*, 71st ed. (CRC, Boca Raton, FL, 1990).
[121] K. M. Ervin and W. C. Lineberger, J. Phys. Chem. **95**, 1167 (1991).
[122] R. D. Mead, U. Hefter, P. A. Schulz, and W. C. Lineberger, J. Chem. Phys. **82**, 1723 (1985).
[123] H. B. Pedersen, C. Brink, L. H. Andersen, N. Bjerre, P. Hvelplund, D. Kella, and H. Shen, J. Chem. Phys. **109**, 5849 (1998).
[124] P. Rosmus and H.-J. Werner, J. Chem. Phys. **80**, 5085 (1984).
[125] D. M. Neumark, K. R. Lykke, T. Andersen, and W. C. Lineberger, Phys. Rev. A **32**, 1890 (1985).
[126] G. J. Schultz, Rev. Mod. Phys. **45**, 423 (1973).
[127] P. A. Schulz, R. D. Mead, P. L. Jones, and W. C. Lineberger, J. Chem. Phys. **77**, 1153 (1982).
[128] E. de Beer, Y. Zhao, I. Yourshaw, and D. M. Neumark, Chem. Phys. Lett. **244**, 400 (1995).
[129] L.-S. Wang, C.-F. Ding, X.-B. Wang, and J. B. Nicholas, Phys. Rev. Lett. **81**, 2667 (1998).
[130] See, e.g., Y. Hahn, in *Recombination of Atomic Ions*, edited by W. G. Graham, W. Fritsch, Y. Hahn, and J. A. Tanis, Vol. 296 of *NATO Advanced Study Institute Series B: Physics* (Plenum, New York, 1992), p. 11.
[131] See, e.g., J. B. A. Mitchell, Phys. Rep. **186**, 216 (1990).